Multi-outrigger-bow Marine Heat Flow Instrument: Measurement Technique

by

S. Nagihara[1,2], L.A. Lawver[1], B. Della Vedova[3],
J.G. Sclater[1,2], K.H. Griffiths[1], and M. Wiederspahn[1]

Institute for Geophysics
The University of Texas at Austin
8701 N. Mopac Blvd.
Austin, Texas 78759

1 Institute for Geophysics, The University of Texas at Austin
2 Department of Geological Sciences, The University of Texas at Austin
3 The University of Trieste, Trieste, Italy

University of Texas Institute for Geophysics Technical Report No. 103

March , 1990

TABLE OF CONTENTS

ABSTRACT

We have developed a marine heat flow probe that combines precision with efficiency of measurement. It consists of 2 to 4 outrigger-bows, each 1.5 m in length and 6.4 mm in diameter, spirally mounted on a 3.5- to 6-m-long strength member. Each outrigger-bow contains four equally spaced thermistors and a heater wire that uses the pulse heating method to measure in-situ thermal conductivity. As presently configured, the thermistors are spaced either 25 or 30 cm apart. The use of multiple sensor strings allows for more thermistors than previous probe designs without requiring a thick sensor tube. The thin sensor string enables a faster thermal response at penetration and reduces the necessary heat pulse power for the thermal conductivity determination. The accuracy of the heat flow data is statistically improved with the increased number of individual temperature measurements and the short, thin outrigger-bow has less thermal contact resistance to the sediments during penetration than the longer (4 to 7 m) violin-bow sensor string. The short sensor strings also allow for easy assembly of the equipment. The electronics package for our instrument (ARGUS II) records 16 thermistors, 2 reference resistors, a water temperature thermistor, the pressure (depth), and the tilt for each data cycle. All the data are stored on RAMs, which are battery backed-up. The resolution of the temperature measurement is approximately 0.5 m^{o}C. The temperature data from 4 selected thermistors and the tilt are transmitted in real time to the ship by an acoustic link.

INTRODUCTION

Marine heat flow instrumentation has improved dramatically during the last decade since in-situ thermal conductivity measurements were combined with multi-penetration thermal gradient measurements (e.g., Hyndman et al., 1979). Even so, there is still a need for more accurate heat flow data (accuracy of less than a few percent), as modern marine heat flow studies have become more and more quantitative (e.g., Davis et al., 1984; Von Herzen et al., 1989; Lister et al., 1989).

Currently, two kinds of multi-penetration marine heat flow instruments are in use. The first is the Ewing type probe, which has several individual outrigger thermistor sensors mounted on a strength member (e.g., Jemsek et al., 1985). The other is the "violin-bow" design developed by C. Lister, which has a single long sensor string that contains several thermistors and is fixed on a strength member at both ends (Hyndman et al., 1979; Davis et al., 1984; Lister et al., 1989). The Bullard probe, which consists of only a single long sensor string, is generally not used for multi-penetration measurements because of the mechanical weakness although it was the first probe developed for marine heat flow measurement (Bullard, 1954).

Since the 1960's, the Ewing type probe has been widely used for thermal gradient measurements (Gerald et al., 1962; Lister 1963). Louden and Wright (1989) showed that more than half of all existing marine heat flow data were measured by this type of probe. The advantages of the Ewing type probe are: (1) the relatively thin outrigger sensor (3 mm O.D.) yields a fast thermal response after the penetration and enables quick measurements, (2) mobilization and assembly of the equipment are relatively easy, (3) the outrigger sensors can also be installed on a piston core barrel so that the thermal conductivity of the recovered sediments can be measured at the same station (this technique, unfortunately, does not allow multiple penetrations). Jemsek et al. (1985) added capability of in-situ conductivity measurement to the Ewing type probe. They used the needle probe technique (Von Herzen and Maxwell, 1959) to measure the in-situ thermal conductivity. The outrigger sensor contains a thermistor and a heater wire and heats up the surrounding sediments for a few minutes. The thermal conductivity is calculated from the way

sediment temperature rises. Von Herzen et al. (1989), developed an Ewing probe with longer (1 m) outrigger sensors. Each sensor contains nine thermistors, but only records the average temperature of the nine thermistors.

Although the Ewing design has been widely used, there are some disadvantages. The number of individual outrigger sensors is generally limited to 6 or 8 because the assembly of the connectors and cables become unwieldy if more sensors are attached. The cables are also vulnerable to damage during frequent penetration. In addition, the in-situ thermal conductivity measurement requires a separate heater circuitry for each outrigger, and that quickly consumes battery power.

The violin-bow probe, which has been used since the late 1970's, offers a more densely spaced thermistor array than the Ewing type probe by utilizing a long sensor string. The probe makes use of the pulse heating method for in-situ thermal conductivity measurements (Lister, 1979). An intense heat pulse of 10 to 20 seconds is applied by the sensor string to the sediment. The conductivity is calculated by the temperature decay in the sediments after the heating. This method requires less battery power and has the further advantage that one can check the self-consistency of the conductivity measurement by comparing the equilibrium temperatures, which are extrapolated from the frictional decay after the penetration and from the decay after the heat pulse (Louden and Wright, 1989).

The violin-bow sensor string is much thicker (8 to 11 mm O.D.) than the outrigger sensor of the Ewing probe because all the thermistors and heater wires go through the single tube, and because the long sensor string requires more mechanical strength than the Ewing probe. The relatively thick sensor string produces a slower thermal response. In addition, the actual penetration of the violin-bow sensor string seems to induce a thermal barrier of water between the sensor string and the surrounding sediment as the long sensor string is pulled through the same column of sediment (Villinger and Davis, 1987a; Hutchison and Owen, 1989). This barrier seems to affect the thermal conductivity determination since there is a significant time delay between the heat pulse and the associated temperature rise of the thermistors. Hyndman et al. (1979) and

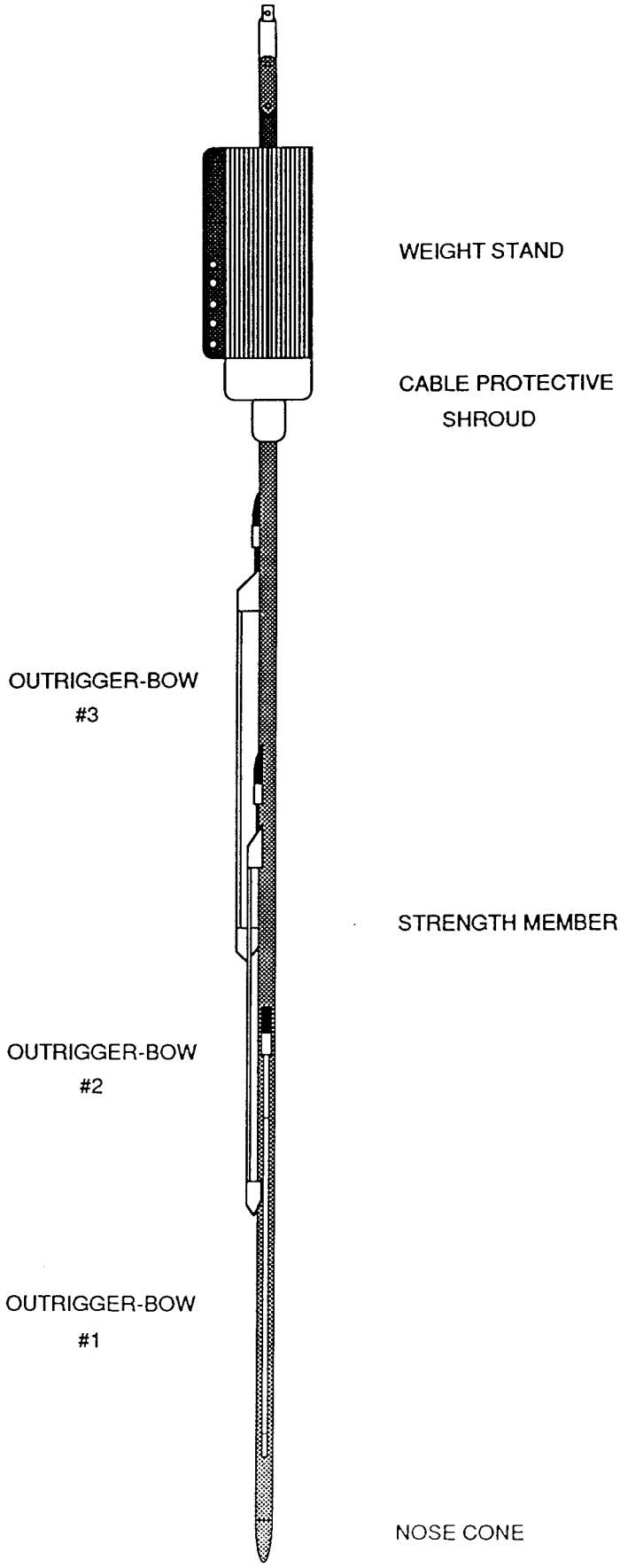

Fig. 1 Schematic diagram of the multi-outrigger-bow heat flow probe.

Villinger and Davis (1987a) have developed a data reduction scheme to cancel this delay by shifting the origin time of the observed heat pulse. Their results show that as great as 30 seconds of shift is necessary for the uppermost thermistor whose adjacent sediments are most likely to have been disturbed by the penetration.

In this study, we present a new marine heat flow instrument that we have named the "multi-outriger-bow probe". We describe both the mechanical and electrical design and the heat flow measurement technique. We will also discuss the accuracy of the new instrument based on actual measurements that we collected during the PD IV-89 cruise to the King George Basin, off the Antarctic Peninsula.

MULTI-OUTRIGGER-BOW HEAT FLOW PROBE

1.Overview

The new heat flow probe (Fig. 1) consists of from two to four sensor strings of intermediate length (1.5 m) (= outrigger-bow) that are spirally mounted on a strength member similar to the Ewing probe. Each sensor string contains four equally spaced thermistors and a long heater wire. The in-situ thermal conductivity of sea floor sediments is measured by the pulse heating method.

With the use of multiple sensor strings of intermediate length instead of a single long sensor string, the probe allows for more thermistors than the violin-bow probe without requiring a thick sensor tube. The thin sensor string (6.35 mm O.D.) enables a faster thermal response at penetration while the increased number of individual temperature measurements statistically improve the accuracy of the heat flow data. The thin sensor string is also advantageous in that it reduces the necessary heat pulse power for the thermal conductivity determination although each sensor string requires an independent heat pulse circuitry. The intermediate length sensor string minimizes the pull through length in the same column of the sediments at penetration and hence, reduces the thermal contact resistance to the surrounding sediments.

2. Mechanical Design

All of the mechanical design and manufacture of the probe were done at the Institute for Geophysics and at the Department of Geological Sciences of the University of Texas at Austin. A detailed description of the mechanical design is given in the Part B of this study (Nagihara et al., 1989). All the electronics are housed in two cylindrical aluminum pressure cases that fit vertically in the weight stand. The weight stand consists of 4 steel pipes (7" O.D., 6" I.D.) welded together (Fig. 2). Two of them accommodate the pressure cases and the other two are partially filled with lead for extra weight. A collar on the bottom of the weight stand holds the strength member. The strength member is made of standard 8.9 cm (3.5") O.D. oilfield drill pipe. The appropriate

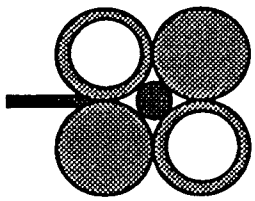

CROSS SECTION

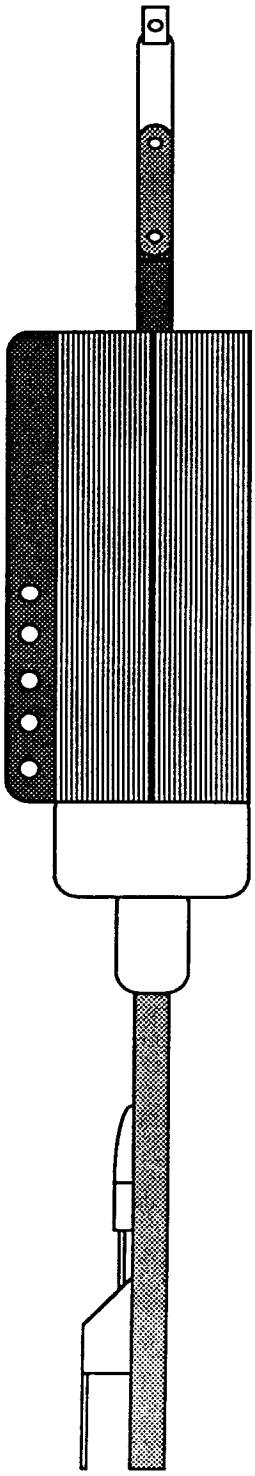

SWIVEL

WEIGHT STAND

CABLE PROTECTIVE SHROUD

STRENGTH MEMBER

Fig. 2 Schematic diagram of the weight stand.

length of pipe is chosen depending on the number of the outrigger-bows (sensor strings) to be used: 3.4 m for 2 bows, 4.4 m for 3 bows, and 5.4 m for 4 bows. Underwater electrical cables are fed through the strength member and connect the sensor strings to the bottom of the pressure cases. The cables are protected by a steel cover on the bottom of the weight stand.

The sensor string is made of 6.35 mm (0.25") O.D., 4.6 mm (0.18") I.D., type-316 stainless steel tubing. Each sensor string is attached to the strength member by a fin (10 cm height) at each end (Fig. 3). The fins are mounted 115 cm apart and the ends of the sensor string are bent along the fins. Thickness of the fins is the same as the diameter of the sensor string so that the probe minimizes the disturbance of sediments at penetration. The bottom end of the sensor string is terminated by a Swagelok^{TM} pressure fitting plug. The upper end is connected to the underwater electrical cable through a small pressure housing.

Each sensor string has four equally spaced (25 cm) thermistors and one heater wire. The heater wire is a polymide varnish coated 90 alloy of 28 AWG (0.321 mm diameter). It has a very low temperature coefficient of resistance (450 ppm/^{o}C). The thermistors we used are YSI 44032, 30 kΩ at 25 ^{o}C (Yellow Springs Inc.). Each electrical wire is teflon coated for insulation. In addition, the whole thermistor and heater wire assembly is placed in a protective fiberglass sleeving to ensure electrical insulation from the wall of the stainless steel tube. The tube is then filled with silicone oil to obtain good thermal contact between the thermistors and the tube wall.

3. Electrical Design

The electronics for our heat flow probe (ARGUS II) were developed at Applied Microsystems Ltd., Sidney, B.C., Canada (Hudson et al., 1989). The data logging circuitry is housed in one pressure case while the thermal conductivity heat pulse and acoustic link circuitry is in the other. Each circuitry system has its own batteries contained in the same pressure case. The batteries are rechargeable with the pressure cases closed.

A block diagram for the system is shown in Fig. 4. The complete system is controlled by an HD64180 micro-processor (Hitachi). Sixteen thermistors, two reference resistors, a water

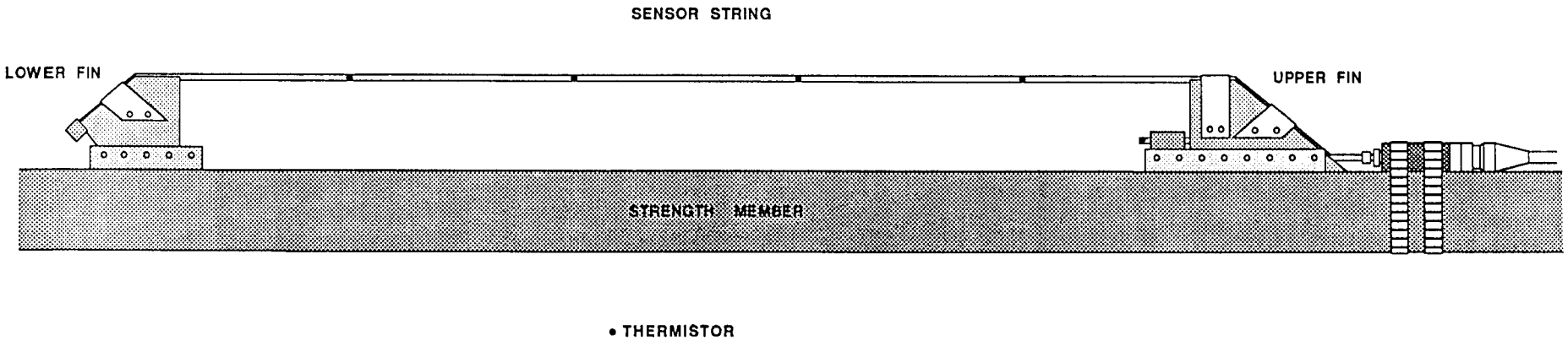

Fig. 3 Assembly of the outrigger-bow.

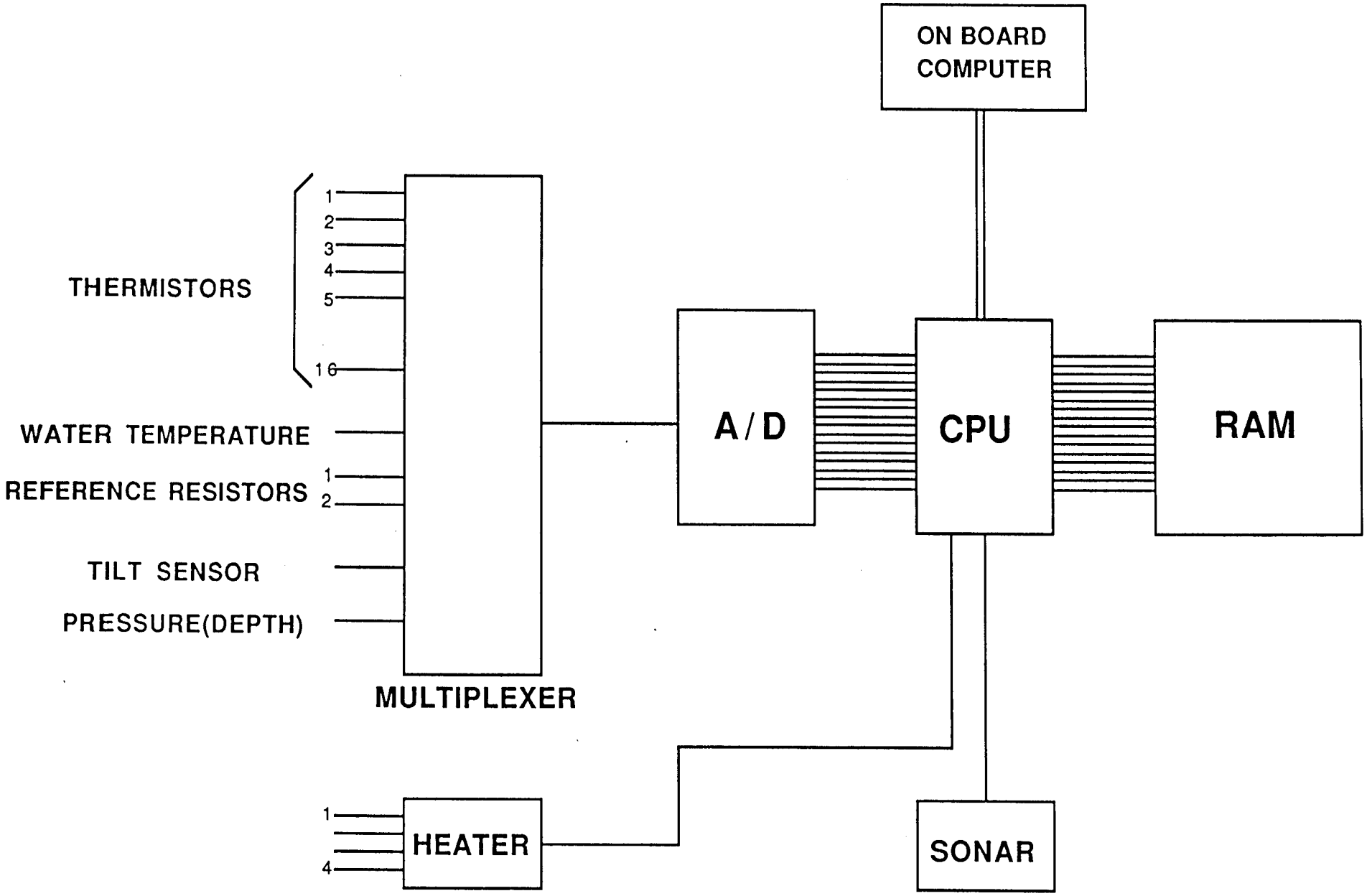

Fig. 4 Block diagram of the ARGUS II electronics.

temperature thermistor, pressure (depth), and tilt are measured and recorded on each sampling cycle. The data sampling rate is software selectable from 10 seconds to 1 hour. The data are stored on RAMs which are battery backed-up and can be retrieved when the instrument is brought back on board. The RAM capacity is 352 K bytes, which is large enough for 20 hours of continuous measurement with a sampling interval of 10 seconds. An RS-232 port is used for communication between the system and the on-board computer. A 12 KHz acoustic link transmits 4 of the 16 thermistor data and the tilt in real time. A temperature measurement resolution of approximately 0.5 m^{o}C is obtained by assigning 16 bits to the temperature range from -2 ^{o}C to 30 ^{o}C.

The heat pulse circuitry uses a constant current regulator for the power supply. Either 4 or 10 A is selected by a hardware switch. The typical heat energy output for our sensor string is expected to be 400 - 600 J/m since the thicker violin-bow sensor string requires 500 to 700 J/m (Hyndman et al., 1979). At a current of 4 A, our sensor string requires 6 to 10 sec. of the heat pulse duration to produce such heat. The duration of the heat pulse should be minimized according to measurement theory. The power source for the heater wire must be capable of high voltage and/or high current because if the power is limited, a long pulse duration is necessary. Our short sensor string is more advantageous than the long violin-bow sensor string from this point of view. The long sensor string requires a higher voltage power or a longer heat pulse duration for the same current since the voltage is proportional to the resistance of the heater wire. For example, a typical violin-bow sensor string of 4 to 7 m length and 10 mm diameter requires a 14 to 24 sec.-long heat pulse (Hyndman et al., 1979; Mojesky, 1981) even with a 10 current. Thus, our thin and short sensor string can produce a more intense heat pulse with less battery power.

HEAT FLOW MEASUREMENT TECHNIQUE

1. Background

The actual measurement technique for the multi-outrigger-bow instrument is the same as that for the violin-bow probe. A record of temperature versus time for a typical heat flow measurement is shown in Fig. 5-a. The probe is lowered from the ship. Prior to penetration, it stops at about 50 meters above the seafloor (Fig. 5-b) to record the bottom water temperature. It is assumed that the bottom water is isothermal for several meters range. Then, the probe is pulled up to 70 meters above the seafloor and is dropped at high speed into the bottom sediments. The frictional heat of penetration causes the sediment temperature to rise almost instantaneously and it then gradually cools down. The temperature record during the frictional decay is used to extrapolate the equilibrium temperature of the sediment. In Fig. 5-a, the frictional temperature decay is not readily apparent because the heat flow at this station is so high (184 mW/m^2). Seven minutes after penetration, the heat pulse is fired for the thermal conductivity determination. The thermal conductivity is calculated from the thermal decay data after the heating. The probe is pulled out of the bottom after several more minutes.

2. Theory

The theory behind the violin-bow probe heat flow measurement has been described in detail by Lister (1979) and Hyndman et al. (1979). Villinger and Davis (1987a) developed a data reduction algorithm that can be done automatically on a micro-computer. Lister et al. (1989) further refined the data reduction scheme to ultimately obtain an absolute accuracy of less than a few percent for their heat flow measurements in the western Pacific.

There are basically three steps required in order to obtain the heat flow value from the temperature values recorded during the probe penetration (Fig. 5-a):

1. Calculate the equilibrium temperature for each thermistor.

2. Calculate the thermal conductivity at each thermistor.

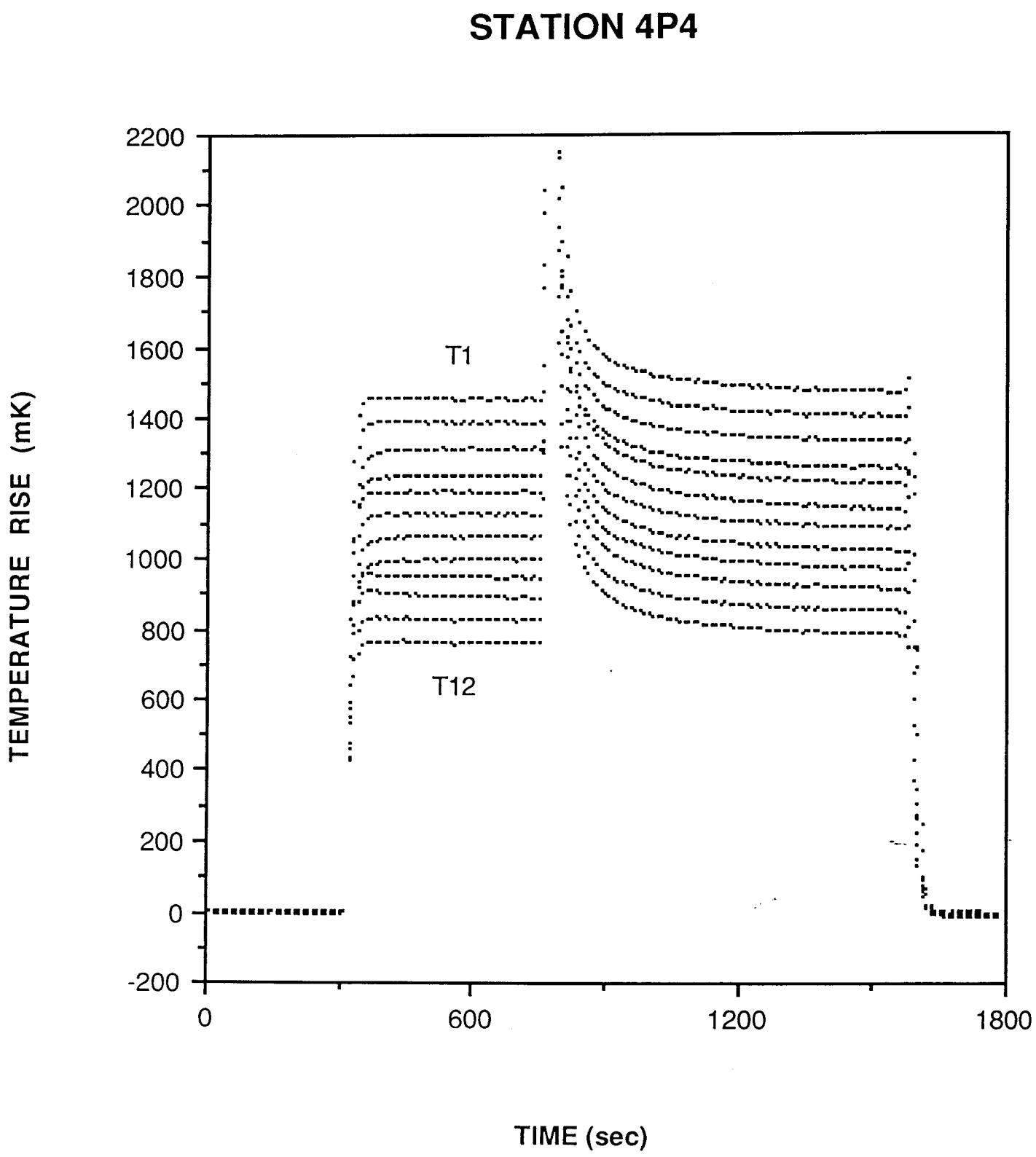

Fig. 5-a Temperature vs. time record for a typical heat flow penetration (Station4p4).

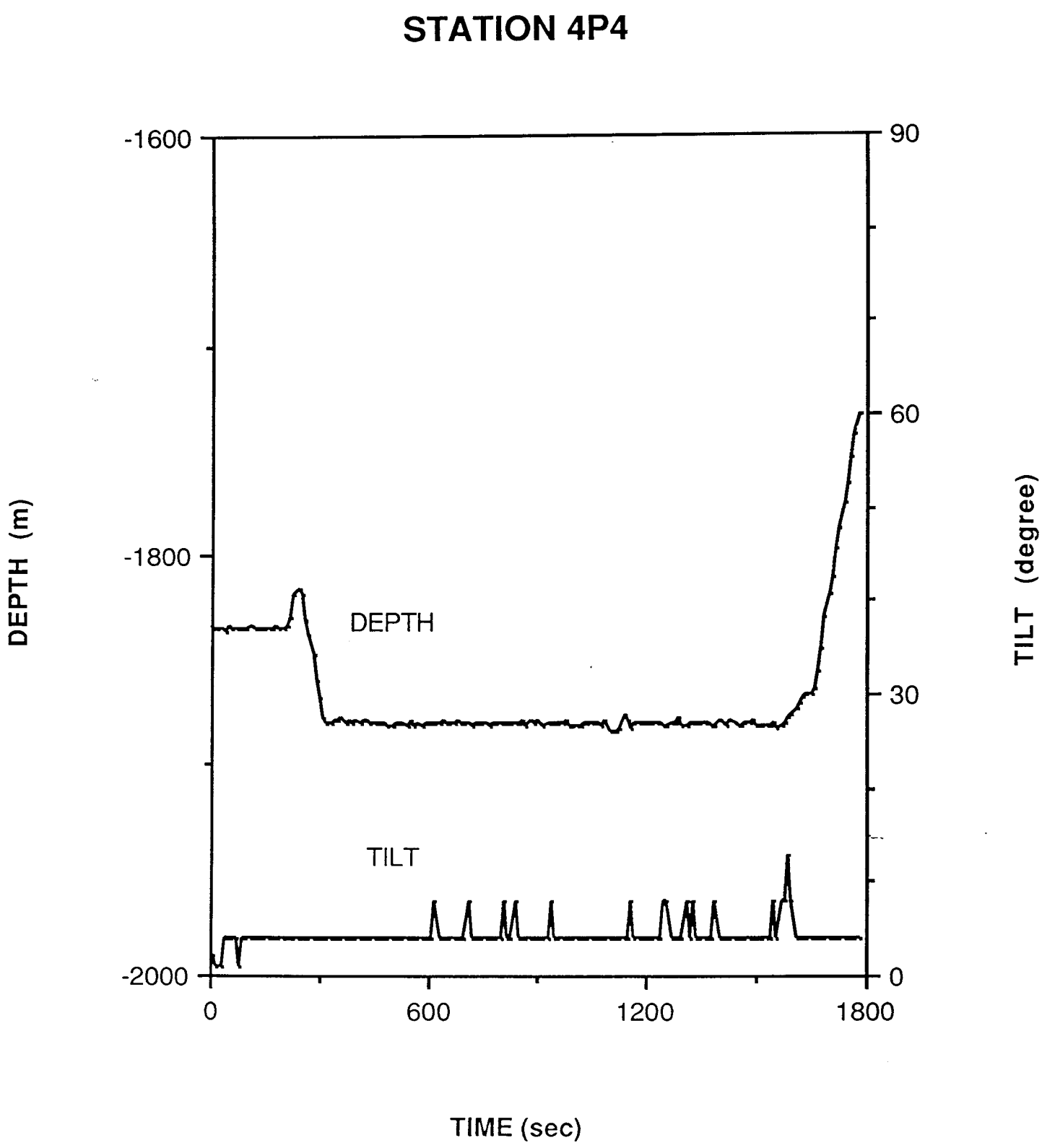

Fig.5-b Tilt and depth vs. time record for a typical heat flow penetration (Station4p4).

3. Calculate the heat flow from the temperature and the thermal conductivity data.

The first two steps are actually inter-related.

Equilibrium temperature of the sediment

The temperature of a cylindrical probe at a time t after penetration should be governed by the following equation (Bullard, 1954):

$$T(t)=T_e+T_0F(\alpha,\tau) \qquad (1)$$

where

$$F(\alpha,\tau) = \frac{4\alpha}{\pi^2} \int_0^\infty \frac{\exp(-\tau u^2)\, d\upsilon}{\upsilon\ \Delta u}$$

and

$$\Delta u=[uJ_0(u)-\alpha J_1(u)]^2+[uY_0(u)-\alpha Y_1(u)]^2$$

J_n and Y_n are Bessel functions of the order n of the first and second kinds. T is the temperature as a function of time. T_e is the equilibrium temperature, which is T of infinite time. T_0 is the temperature rise produced by the frictional heat at the penetration. α is twice the ratio of the heat capacity of the measured sediment to that of the probe ($\alpha=2\pi a^2\rho c/S$). a is the probe radius, ρ and c are density and specific heat of the sediment, respectively, and S is the heat capacity of probe. τ defines the thermal time constant of the probe in the sediment with thermal diffusivity κ ($\tau\equiv\kappa t/a^2$). It is assumed that the probe is a perfect thermal conductor and that the temperature rise by the frictional heat is instantaneous.

Since α is defined by the thermal properties of the sediment and the probe, it is constant for each thermistor, but may vary from one to another. Hence, $F(\alpha,\tau)$ for each thermistor is merely a function of τ and is approximately inversely proportional to τ (Blackwell, 1954). τ is proportional to t since κ/a^2 is constant for each thermistor. Therefore, when t is infinity, $F(\alpha,\tau) = 0$. One can

obtain T_e by plotting the frictional temperature decay data (T) as a function of $F(\alpha,\tau)$ and calculating the intercept temperature.

Calculation of $F(\alpha,\tau)$ requires knowledge of ρc and κ. Since $\kappa=K/\rho c$, where K is the thermal conductivity, κ cannot be obtained without K. Thus, it turns out that one has to know the thermal conductivity to calculate the equilibrium temperature .

Thermal conductivity of the sediment

Equation (1) is also applicable to the heat pulse thermal decay assuming that the heating is instantaneous. For simplicity, we set $T_e = 0$ so that,

$$T(t)=T_0F(\alpha,\tau) \qquad (2)$$

In this instance, t is now the time after the heat pulse and T_0 is the temperature rise caused by the heat pulse. We assume that the heat pulse is a delta function in time because the temperature rise is assumed instantaneous. The only difference from the case of frictional decay is that we know the amount of the energy input by the heat pulse. The temperature of the probe rises instantaneously at t=0 to T_0, which should be equal to Q/S where Q is the total heat input.

For large τ (> 10), $F(\alpha,\tau)$ can be approximated by

$$F(\alpha,\tau)=1/(2\alpha\tau) \qquad (3)$$

and when $\alpha = 2$, the best approximation is found (Hyndman et al., 1979). Considering $T_0 = Q/S$ and by substituting (3) into (2), (2) can be written as

$$T(t) = Q/(4\pi Kt) \qquad (\tau > 10) \qquad (4)$$

Thus, K is obtained as

$$K = Q/(4\pi tT) \qquad (5)$$

though eq. (5) is valid only if τ is very large.

In order to use the data for $\tau < 10$, typical of marine heat flow measurements, a correction factor: $C(\alpha,\tau) = 1/[2\alpha\tau F(\alpha,\tau)]$ is applied to T,

$$T_c(t) = T(t)C(\alpha,\tau) \qquad (6)$$

Then,

$$T_c = Q/(4\pi Kt) \qquad (7)$$

This equation is valid for any $t > 0$.

Calculation of $C(\alpha,\tau)$, again, requires knowledge of ρc and κ. For ocean sediments, empirical relationships exist among ρc, κ, and K (e.g., Von Herzen and Maxwell, 1959; Ratcliffe, 1960; Hyndman et al., 1979; Lister et al., 1989). Thus, if one of them is known, the other two can be estimated. Then, T_e and K are calculated iteratively: [1] ρc and κ are obtained by empirical relationships assuming a realistic K, [2] $F(\alpha,\tau)$ is calculated, [3] T_e is obtained from T vs. $F(\alpha,\tau)$ plot, [4] $C(\alpha,\tau)$ is calculated, [5] T_c vs. 1/t plot is obtained, [6] a new K is calculated from the plot by eq. (7), and [7] if the new K is different from the previous K, the same process is repeated by replacing the old K with the new K. The value for K generally converges within 3 or 4 iterations (Hyndman et al., 1979). The final K is the true thermal conductivity and T_e calculated from the final K is the true equilibrium temperature.

There is a simplified computation method assuming that α is constant. For ocean sediments, α actually ranges from 1.7 to 2.3 for typical violin-bow probe construction. Theoretically, α should be reevaluated for the assumed K for each iteration. However, for simple calculation, α can always be fixed at 2.0 (Hyndman et al., 1979; Villinger and Davis, 1987a) since K is not very sensitive to variation of α. The introduced error in the K determination is 3 - 4 % in this α range (Lister et al., 1989). When the accuracy of the data is more critical, the error should not be neglected.

In this study, we used a fixed α for simplicity. For our sensor string, ρc is estimated to be 3.1×10^6 J/m^{3}K: 50% stainless steel($\rho c = 4.0 \times 10^6$ J/m^{3}K) and 50% probe contents ($\rho c = 2.1 \times 10^6$ J/m^{3}K) (see Lister, 1979 for the ρc values). For marine sediments, ρc is 3.3×10^6 to 3.6×10^6. Therefore, we chose $\alpha = 2.2$ for our probe.

In reality, the probe is not a perfect conductor. It is never heated up instantaneously in the form described by eq. (2). There is a certain amount of time delay associated with heat conduction form the internal probe to the outside sediment and vice versa. Another problem with the measurement theory is that the heat pulse is not a perfect delta function in time. It takes 14 - 24

sec. for the regular violin-bow probes and 6 - 10 sec for our outrigger-bow probe to input the heat pulse. These drawbacks can be canceled by finding the effective origin time for the heat pulse, which is often later than the actual firing time. Villinger and Davis (1987a) introduced a data reduction algorithm that shifts the observed origin time so that eqs. (2) and (7) are valid for the data. They suggested that the measurement error can be reduced to less than 1 % by this method.

Determination of the heat flow value

If the thermal conductivity of the sediments is uniform, the thermal gradient is linear and the heat flow is a simple product of the thermal conductivity and the thermal gradient. However, in most cases, the conductivity varies with depth. The heat flow value is determined from a so-called "Bullard plot" when the in-situ thermal conductivity is available for each thermistor. The Bullard plot is a plot of temperature versus depth divided by thermal conductivity (Bullard depth). This method was originally used for heat flow measurements on deep bore holes on land where large variation of thermal conductivity is observed (Bullard, 1939).

Mathematically, the definition of heat flow q is q=KdT/dz where z is the depth. It can also be written as

$$\int_0^z dT = q\int_0^z \frac{dz}{K} \qquad (8)$$

Thus, the heat flow is obtained as the slope of Bullard plot.

3. Operation at sea

Our heat flow instrument was extensively tested on the PD IV-89 cruise of R/V Polar Duke to the King George Basin, off Antarctic Peninsula. We made 54 penetrations including 22 where the heat pulse fired (Nagihara and Lawver, 1989). The sea floor of the survey area is flat and covered by thick sediments. The sediments were mostly soft mud and were an excellent environment for penetration of the heat flow probe. Three outrigger-bows (= 12 thermistors) were attached to the strength member. We tested two different sensor spacings; the bottom bow

(#1) had a 30 cm interval between the thermistors and a distance of 15 cm between the fins and the uppermost and lowermost thermistors; the middle (#2) and upper bow (#3) had a 25 cm thermistor interval and a 20 cm offset from the fins. In addition to the heat flow measurements, we took four piston cores in the basin for on board thermal conductivity measurements.

4. Data reduction

For our data reduction, we adopted HFRED (Villinger and Davis, 1987b), which is a computer program based on the algorithm developed by Villinger and Davis (1987a). The program is widely used for the violin-bow instruments because of its simple data formatting and quick computation on a personal computer. It uses the fixed α method (see the previous section). The data reduction scheme developed by Lister et al. (1989) is more precise in that it uses the variable α method. However, architecture of the program is somewhat dependent on the electrical design of the instrument they used and requires a longer computation time. Thus, we used HFRED for simplicity. We modified the program so that the thermistor intervals and the power of the heat pulse can be different among the different sensor strings.

The results for a typical heat flow penetration are shown in Fig. 6 and Table 1. Frictional temperature decay vs. $F(\alpha,\tau)$ (Fig. 6-A), heat pulse decay vs. $F(\alpha,\tau)$ (Fig. 6-B), temperature and thermal conductivity vs. depth (Fig. 6-C), and Bullard depth (depth/thermal conductivity) vs. temperature (Fig. 6-D) are plotted for the same station we showed in Fig. 5. The print-out from the program is also shown in Table 1. The temperature data for τ between 2 and 10 were taken for the frictional and heat pulse decay plots. The actual temperature, depth and tilt records are shown in Table 2. The decay plots for each thermistor show ideal straight lines (Fig. 6), indicating that the thermal characteristics of the probe are appropriate. Thermistors 1 and 4 are closer to the fins (15 cm apart) than are Thermistors 5, 8, 9 and 12 (20 cm apart). However, the distance seems large enough to avoid thermal effects from the fins.

In this study, the heater power (Q) may not be as accurate as it should be. The battery power for the heat pulse was not strong enough to maintain the necessary current when the heater

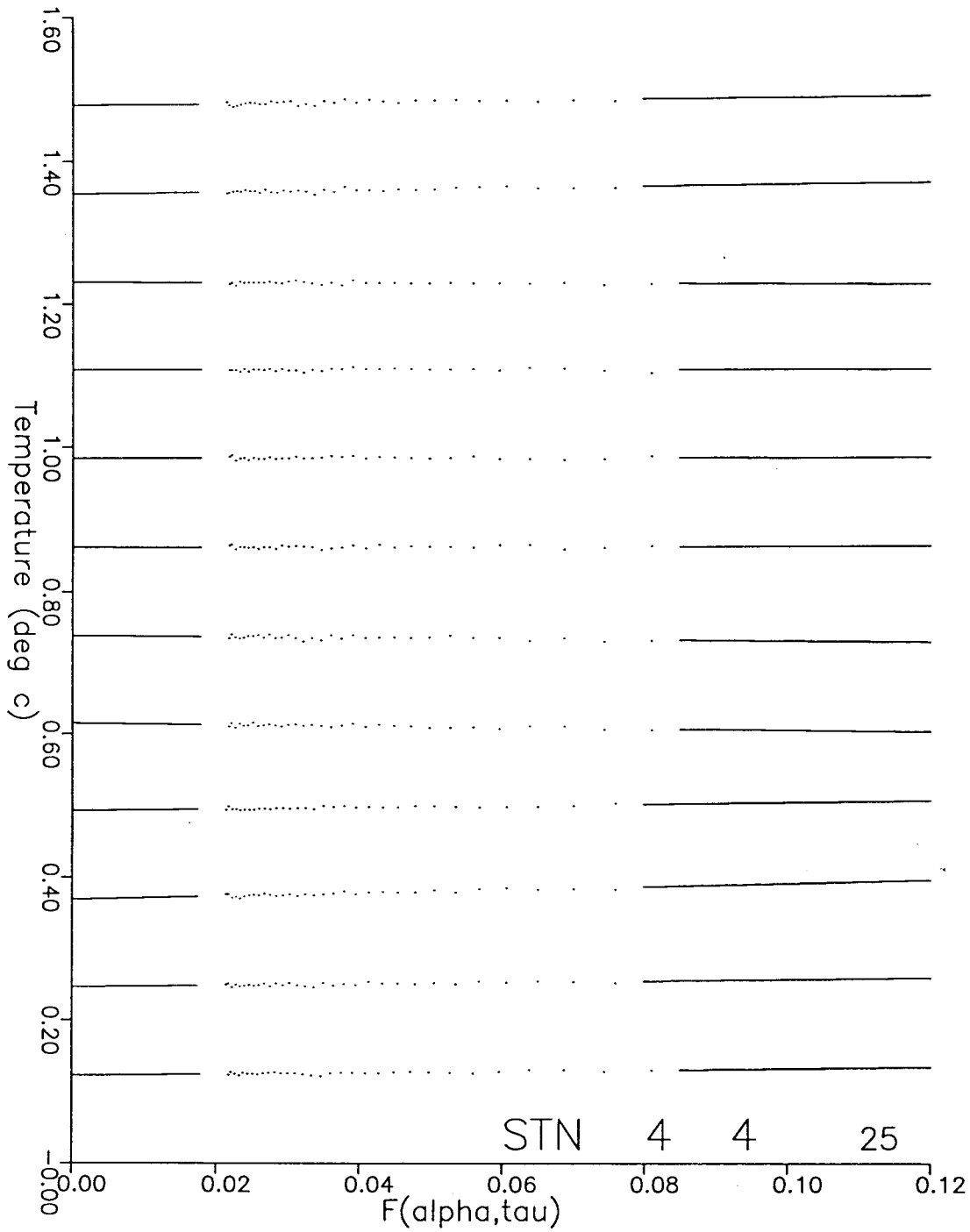

Fig. 6-A Frictional decay vs. F(α,τ) plot for Station4p4.

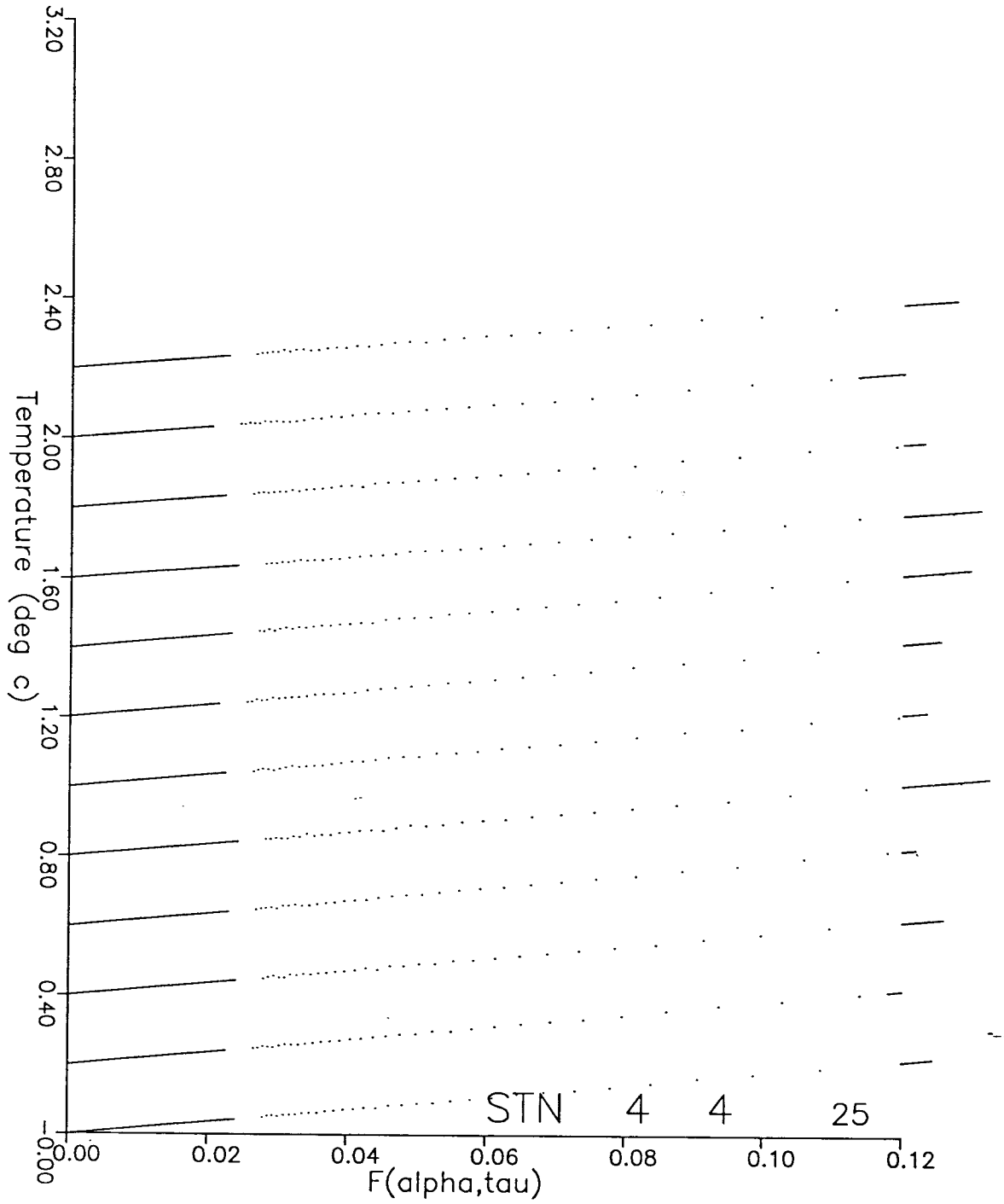

Fig. 6-B Heat pulse decay vs. F(α,τ) plot for Station4p4.

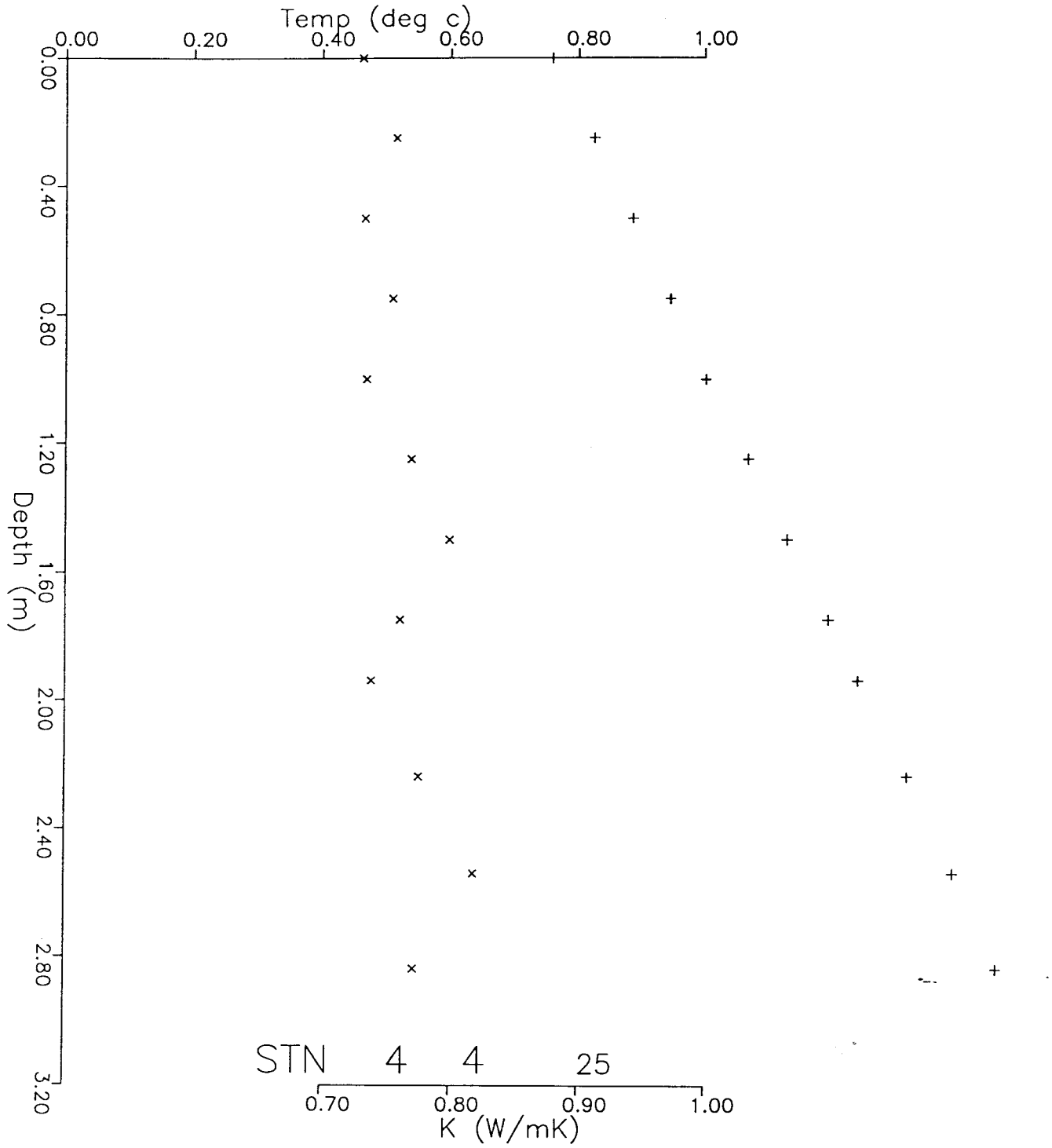

Fig. 6-C Temperature and thermal conductivity vs. depth plot for Station4p4.

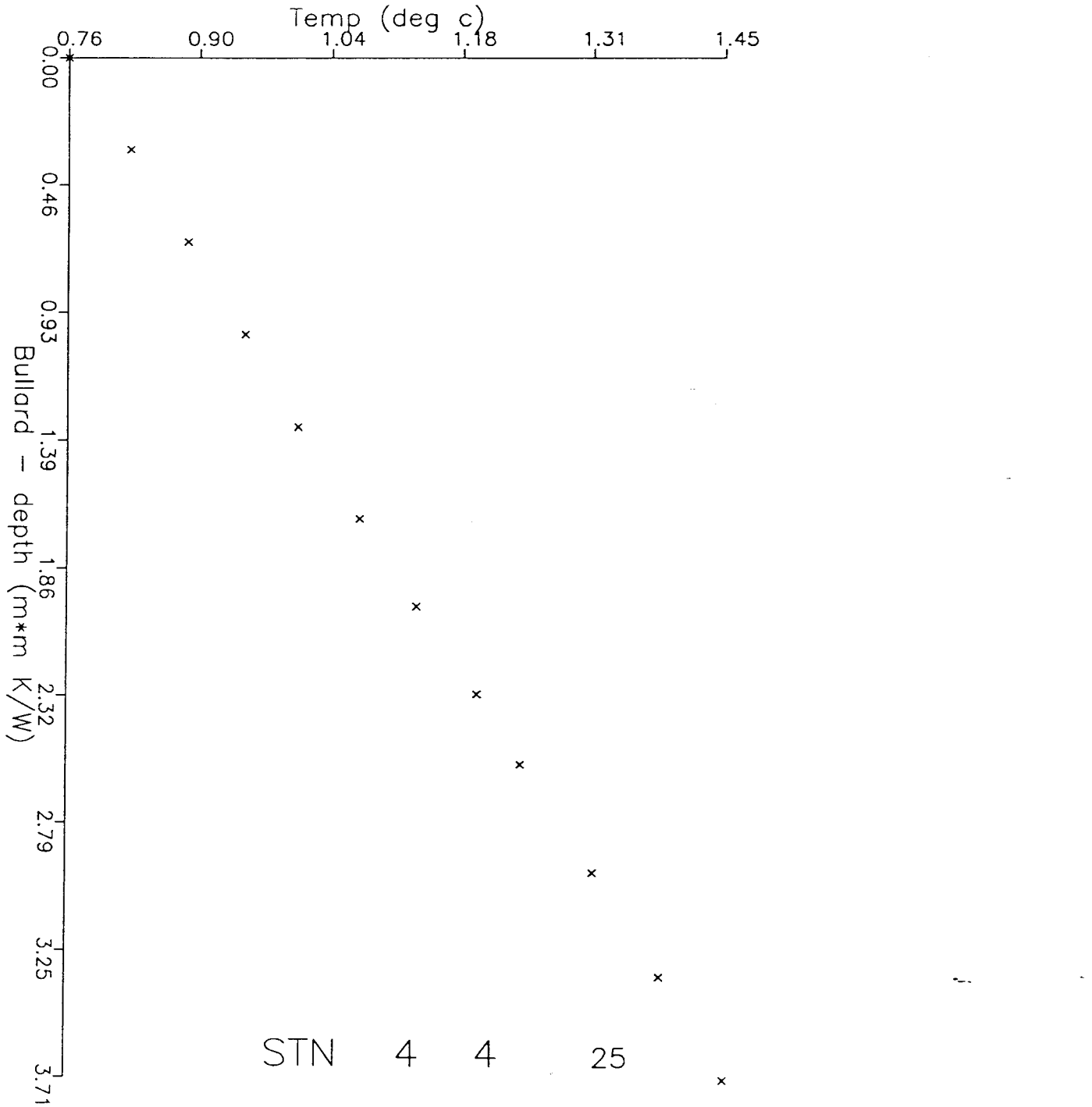

Fig. 6-D Bullard Depth (depth/thermal conductivity) vs. temperature plot for Station4p4.

was on. During experiments in a cold laboratory, we discovered that the actual heater current varied between 3.3 A and 3.7 A while the power circuitry is designed to have a constant current of 4 A. The cold bottom-water temperature (-1.4 °C) that we had, weakened the battery output.

We estimated the actual Q by comparing the thermal conductivity data calculated from the heat pulse decay to those measured on the piston core samples. The thermal conductivities of the core samples were measured by the needle probe technique (Von Herzen and Maxwell, 1959) and corrected for in-situ pressure and temperature based on Ratcliffe (1960). The four piston core stations were widely distributed in the King George Basin. Although the measurements showed a fair amount of scatter (Fig. 7), there seems to be no regional variation. This is also reasonable since we observed uniform surface sediment structure throughout the basin from a detailed 3.5 KHz survey. Thus, we applied the linear least-squares fit to the data, from which apparent outliers and very high thermal conductivity values caused by thin ash layers were excluded. We obtained the thermal conductivity vs. sub-bottom depth relation down to 6 m : $K=0.764+4.64\times10^{-3}Z$, where K is in W/mK and Z is the sub-bottom depth in meters. To compare this relationship to the in-situ thermal conductivity measurements, we first calculated the sub-bottom depths of all the thermistors for 12 arbitrarily selected penetrations. The calculation was based on the super penetration estimation based on thermal gradients of the upper 4 thermistors. Then, we obtained the heater power iteratively for each outrigger-bow by comparing the in-situ thermal conductivity determination to the data from the needle probe measurement. The obtained Q values were fairly consistent among the penetrations (standard deviation of 8 %) while we tested three different pulse lengths (6 sec, 8 sec, and 10 sec).

Table 3 shows heat pulse origin time shifts necessary to validate eq. (7). Here, the shift is from the center of the pulse. Three different pulse lengths were tested. Although the 10 sec. pulse (Q=260.1, 299.6 J/m) was tested for only one penetration, the shifts are significantly smaller than those for the other two cases. The shifts for the 8 sec. pulse (Q=208.0, 239.7, 251.6) are slightly smaller than those for the 6 sec. pulse (Q=156.1, 179.7, 188.7). The shifts for the 6 and 8 sec. pulses are not much smaller than those reported for the violin-bow probes (15 to 35 sec,

FRICTIONAL DECAY

sensor	no of points total / used	sed.temp. (deg)	95% level error (deg)	gradient (mdeg/m)	delay (s)	slope	water temp.
1	44 / 32	1.452	.0049	225.2	8.5	0.063	-1.501
2	44 / 32	1.385	.0040	234.5	8.5	0.095	-1.384
3	44 / 32	1.314	.0034	257.7	1.0	-0.062	-1.395
4	44 / 32	1.237	.0038	191.6	1.0	-0.027	-1.442
5	44 / 32	1.191	.0037	257.4	1.0	-0.023	-1.457
6	44 / 32	1.127	.0040	241.7	1.0	-0.010	-1.426
7	44 / 32	1.067	.0048	263.3	1.0	-0.099	-1.453
8	44 / 32	1.001	.0036	243.3	1.0	-0.122	-1.511
9	44 / 32	0.946	.0027	238.8	8.5	0.101	-1.380
10	44 / 32	0.886	.0034	244.8	8.5	0.214	-1.445
11	44 / 32	0.825	.0036	261.3	8.5	0.100	-1.421
12	44 / 32	0.759	.0032	0.0	1.0	0.094	-1.434

Heat Pulse Decay

sensor	no of points total / used	temp. at infinity (deg)	conductivity(W/mK)	sd (W/mK)	delay (s)	slope	ci ti
1	73 / 32	0.0000	0.772	.002	-25.7	1.52	3 15
2	73 / 32	0.0002	0.819	.002	-21.1	1.56	3 11
3	73 / 32	-.0001	0.776	.002	-23.1	1.53	3 14
4	73 / 32	-.0001	0.739	.002	-24.1	1.50	3 16
5	73 / 32	-.0001	0.761	.002	-25.8	1.74	3 16
6	73 / 32	0.0002	0.800	.002	-27.4	1.78	3 14
7	73 / 32	-.0001	0.769	.002	-22.7	1.76	3 14
8	73 / 32	-.0001	0.735	.002	-24.6	1.72	3 16
9	73 / 32	0.0001	0.755	.002	-19.6	1.82	3 14
10	73 / 32	0.0001	0.733	.002	-19.8	1.80	3 14
11	73 / 32	0.0000	0.758	.001	-17.0	1.82	3 13
12	73 / 32	-.0001	0.731	.001	-18.4	1.80	3 14

Remark : If ci and ti = 0 k = k(initial)
If ci and ti = 99 time < 0

HEAT FLOW RESULTS FOR STA 4 PEN 4

sensor	depth (m)	sed.temp. (deg)	gradient (mdeg/m)	conductivity (W/mk)	Bullard-depth (m*mK/W)	heat flow (mW/m*m)
1	2.87	1.452	225.2	0.77	3.754	178.93
2	2.57	1.385	234.5	0.82	3.379	186.80
3	2.27	1.314	257.7	0.78	3.000	195.02
4	1.97	1.237	191.6	0.74	2.606	143.69
5	1.73	1.191	257.4	0.76	2.284	200.71
6	1.48	1.127	241.7	0.80	1.965	189.58
7	1.23	1.067	263.3	0.77	1.648	197.90
8	0.98	1.001	243.3	0.73	1.316	181.16
9	0.75	0.946	238.8	0.75	1.007	177.61
10	0.50	0.886	244.8	0.73	0.671	182.42
11	0.25	0.825	261.3	0.76	0.336	194.45
12	0.00	0.759	0.0	0.73	0.000	0.00

Notes :
(1) weighting factor for Bullard-depth : 0.0
(2) plot id (0 = no plot) : 72.
(3) assumed conductivities for sensors :

Table 1 Print-out from HFRED.

	time	T1	T2	T3	T4	T5	T6	T7	T8	T9	T10	T11	T12	Depth	Tilt	Water T	Int. T
1	0.0	0.6	0.3	0.7	0.7	-0.8	1.0	0.9	0.1	1.6	0.2	1.1	-0.2	-1833.8	2.0	-1516.9	95.6
2	10.0	2.4	5.0	2.5	1.6	3.9	4.1	3.5	3.1	2.9	3.2	4.2	2.4	-1835.2	2.0	-1515.6	103.7
3	20.0	1.5	-1.0	1.6	0.7	2.6	0.6	2.2	-0.3	-0.5	0.2	0.7	-0.2	-1835.5	1.0	-1520.4	105.3
4	30.0	1.5	3.7	-0.2	0.2	1.3	1.9	-1.2	-0.3	2.9	0.2	-0.6	1.5	-1835.2	1.0	-1518.6	112.3
5	40.0	0.7	0.3	-0.1	-0.1	1.8	0.6	1.8	1.4	-0.1	0.7	1.2	-0.1	-1836.3	4.0	-1516.1	117.7
6	50.0	1.0	-1.9	-1.9	-1.9	0.9	2.3	2.6	0.5	0.3	-0.7	1.1	-0.6	-1834.6	4.0	-1519.9	118.8
7	60.0	-4.1	-1.9	-0.6	-3.6	0.9	0.1	-3.0	0.0	-1.8	-2.8	0.2	-3.6	-1834.9	4.0	-1520.0	119.8
8	70.0	1.9	-1.0	3.3	-0.6	3.9	1.9	-0.3	2.3	-0.5	2.3	-0.1	2.0	-1835.2	4.0	-1517.8	126.5
9	80.0	2.7	-0.6	-1.9	-0.2	2.1	1.4	0.5	-2.5	-2.3	1.4	1.5	0.6	-1836.0	1.0	-1518.2	131.9
10	90.0	0.6	-0.6	-1.4	-0.6	-0.8	-0.3	0.5	-0.8	-1.4	-1.1	-1.5	-3.2	-1834.9	4.0	-1520.4	137.8
11	100.0	1.9	3.7	2.0	-0.2	0.1	3.1	3.9	-1.2	-0.5	2.3	3.3	1.1	-1835.5	4.0	-1519.5	137.3
12	110.0	2.7	4.1	-0.6	3.2	0.9	2.3	2.6	0.5	2.5	1.5	3.7	-1.0	-1834.4	4.0	-1519.0	145.2
13	120.0	-2.4	0.2	-1.5	0.6	-1.3	2.3	0.0	-4.6	-0.1	-2.8	-0.6	-0.2	-1834.9	4.0	-1523.8	147.3
14	130.0	1.5	3.2	0.3	-0.6	-1.2	-0.7	3.1	0.5	-2.2	0.2	0.7	1.1	-1835.2	4.0	-1520.3	149.4
15	140.0	-4.1	-3.6	-3.2	-2.8	-4.7	-1.1	-2.1	-2.5	-2.7	-2.4	0.2	-1.1	-1835.5	4.0	-1518.6	152.8
16	150.0	2.3	3.3	2.4	0.7	0.5	2.7	0.5	2.3	2.5	1.9	4.6	3.2	-1835.5	4.0	-1516.9	159.1
17	160.0	-1.5	-0.6	-2.3	-2.3	-1.2	-3.3	0.5	-0.8	-1.0	-0.3	-0.1	-1.5	-1836.0	4.0	-1520.4	160.6
18	170.0	0.1	-1.5	-0.6	-1.1	0.0	-1.1	-1.7	1.4	-2.3	-0.3	0.2	-0.6	-1835.7	4.0	-1521.6	163.9
19	180.0	0.1	-1.0	-0.6	-0.2	-2.5	-0.3	2.1	-1.2	-0.6	-1.1	-0.2	-0.6	-1834.4	4.0	-1519.1	167.2
20	190.0	0.6	2.0	1.1	1.9	-0.8	1.0	0.1	0.1	0.3	0.2	1.1	0.7	-1834.9	4.0	-1520.3	172.2
21	200.0	-0.7	-1.0	-0.6	-0.6	-0.4	1.0	-1.7	-1.6	0.3	0.2	0.2	-1.5	-1835.5	4.0	-1519.1	177.0
22	210.0	-0.3	-1.0	1.6	0.3	4.3	0.6	0.9	0.1	1.2	0.2	-1.0	1.1	-1834.4	4.0	-1520.3	178.7
23	220.0	0.2	2.4	-0.6	-0.2	-0.8	-1.1	0.1	1.4	0.8	0.6	-0.1	0.6	-1830.3	4.0	-1520.8	179.7
24	230.0	-2.8	-2.7	-2.3	-1.9	-1.7	-2.8	-2.1	-1.6	-1.8	-0.3	1.1	1.9	-1819.4	4.0	-1517.8	185.3
25	240.0	0.6	0.3	-2.3	1.9	1.3	-2.0	0.1	0.9	-1.4	0.6	1.5	-1.5	-1816.4	4.0	-1517.8	183.9
26	250.0	1.9	2.4	2.9	-0.2	3.1	-0.6	3.9	-0.7	3.8	0.2	3.7	-0.1	-1819.4	4.0	-1516.1	187.9
27	260.0	3.2	2.0	-0.6	0.3	3.9	3.6	-0.3	-1.5	-0.5	3.2	4.1	2.4	-1831.1	4.0	-1516.5	195.4
28	270.0	2.7	3.7	3.3	2.8	3.5	2.7	3.1	2.7	2.9	2.8	2.8	-0.6	-1838.2	4.0	-1516.1	196.4
29	280.0	-0.3	0.2	-3.6	-2.3	0.0	-4.1	-2.1	0.9	-1.4	-2.0	1.5	-3.6	-1847.4	4.0	-1521.6	195.2
30	290.0	4.5	-0.6	3.7	2.0	2.2	4.0	-0.3	3.1	1.2	1.1	3.7	1.1	-1859.4	4.0	-1516.1	199.1
31	300.0	4.5	3.3	1.6	0.7	-0.3	2.8	3.9	2.7	2.1	1.9	1.6	1.6	-1868.1	4.0	-1519.4	205.6
32	310.0	1.0	2.0	1.6	1.5	1.8	3.1	3.0	2.6	1.6	2.3	2.8	1.5	-1878.2	4.0	-1519.1	205.3
33	320.0	829.8	643.0	532.9	536.2	724.8	595.5	549.3	474.7	577.0	462.6	431.0	434.6	-1879.8	4.0	-1518.6	207.6
34	330.0	1277.3	1161.9	1052.7	1012.8	1057.2	954.3	878.4	811.5	867.6	789.8	710.6	664.1	-1880.3	4.0	-1516.1	210.5
35	340.0	1404.8	1315.1	1212.6	1158.8	1147.6	1061.5	985.9	916.5	932.3	879.0	792.3	733.6	-1878.4	4.0	-1514.4	212.8
36	350.0	1441.5	1364.8	1265.2	1203.8	1175.3	1098.5	1023.2	956.7	951.2	902.6	820.0	755.7	-1879.5	4.0	-1514.8	215.6
37	360.0	1453.5	1380.9	1289.0	1220.6	1187.1	1113.9	1041.2	973.2	956.1	908.9	829.3	765.1	-1878.2	4.0	-1514.0	216.5
38	370.0	1457.6	1386.9	1297.2	1228.8	1188.9	1118.5	1050.2	979.9	956.6	908.9	830.2	766.4	-1880.1	4.0	-1514.8	218.0
39	380.0	1458.7	1390.2	1303.8	1232.1	1189.4	1120.8	1052.1	983.6	954.4	907.2	833.8	767.3	-1879.2	4.0	-1515.3	220.4
40	390.0	1459.5	1387.9	1303.3	1229.7	1188.9	1123.5	1056.5	988.5	953.0	903.1	831.5	767.3	-1880.9	4.0	-1515.3	223.6
41	400.0	1458.6	1389.3	1307.0	1235.3	1187.1	1127.2	1055.2	989.8	952.6	901.8	832.9	765.1	-1879.2	4.0	-1513.6	223.2
42	410.0	1454.5	1390.2	1308.8	1230.3	1191.7	1127.2	1057.9	989.9	954.9	899.6	830.3	766.9	-1880.3	4.0	-1512.8	228.8
43	420.0	1455.8	1390.6	1307.9	1234.3	1188.0	1124.9	1057.4	990.7	951.7	900.4	832.0	765.1	-1879.2	4.0	-1514.4	232.5
44	430.0	1454.0	1390.7	1311.1	1237.5	1187.1	1123.1	1061.5	995.2	950.3	899.1	832.5	767.3	-1879.2	4.0	-1514.0	231.1
45	440.0	1456.2	1393.7	1310.0	1238.8	1188.9	1129.3	1058.3	996.4	950.7	901.3	830.6	767.7	-1880.6	4.0	-1512.7	237.0
46	450.0	1456.2	1392.8	1311.0	1234.7	1188.9	1128.9	1062.8	992.0	949.8	899.9	832.9	765.1	-1879.8	4.0	-1516.1	240.3
47	460.0	1457.7	1392.0	1311.1	1237.1	1192.2	1126.3	1062.4	994.7	950.3	895.5	828.5	762.4	-1879.8	4.0	-1517.4	239.1
48	470.0	1456.7	1389.6	1311.9	1236.5	1189.8	1126.6	1065.5	994.2	951.6	898.6	830.2	763.3	-1880.1	4.0	-1513.1	243.6
49	480.0	1456.8	1389.3	1311.1	1236.2	1189.4	1127.2	1063.3	994.3	951.7	895.5	828.9	764.2	-1880.1	4.0	-1513.6	245.6
50	490.0	1453.5	1389.7	1311.0	1237.0	1189.8	1127.5	1062.8	996.1	949.8	895.5	829.3	765.1	-1881.7	4.0	-1512.3	249.2
51	500.0	1456.2	1387.3	1311.9	1237.9	1190.7	1126.2	1063.3	996.9	949.4	895.9	829.3	764.2	-1881.4	4.0	-1513.5	250.7
52	510.0	1458.0	1389.2	1311.9	1237.4	1192.1	1130.2	1063.2	998.2	950.7	895.5	831.5	762.8	-1879.8	4.0	-1514.8	253.9
53	520.0	1454.5	1388.8	1311.5	1237.5	1188.9	1124.9	1062.9	995.6	949.9	893.3	827.1	762.9	-1880.6	4.0	-1512.3	256.3
54	530.0	1459.4	1393.3	1316.0	1240.6	1193.4	1129.3	1066.4	1000.0	951.6	896.8	828.4	763.7	-1880.1	4.0	-1509.3	263.6
55	540.0	1454.5	1386.9	1308.3	1237.5	1192.1	1125.8	1061.5	997.4	950.3	893.7	826.7	763.3	-1881.4	4.0	-1512.3	257.8
56	550.0	1456.7	1389.6	1312.8	1237.9	1193.4	1124.8	1066.4	995.1	952.0	893.2	830.2	762.8	-1878.4	4.0	-1510.6	265.1
57	560.0	1450.0	1382.5	1309.4	1235.3	1190.9	1123.1	1059.3	997.1	947.2	891.1	824.0	758.5	-1881.2	4.0	-1515.7	263.1
58	570.0	1452.7	1387.4	1312.0	1236.6	1190.3	1126.7	1062.4	998.3	949.0	893.3	825.4	759.3	-1880.1	4.0	-1514.5	266.7
59	580.0	1450.0	1389.0	1313.1	1232.7	1190.0	1127.7	1058.0	997.5	948.6	890.7	827.2	760.7	-1881.2	4.0	-1514.5	269.2
60	590.0	1457.1	1387.7	1315.5	1236.0	1192.5	1128.4	1062.3	999.1	948.4	893.2	830.1	762.8	-1880.3	4.0	-1514.8	274.9
61	600.0	1455.9	1389.3	1314.3	1235.7	1190.3	1127.6	1066.9	998.3	949.0	891.1	827.1	762.9	-1880.3	4.0	-1508.9	279.8

Table 2 Station 4p4 data corrected for appropriate units; temperature in mili-degree C, depth in meter, tilt in degree (1/3).

	time	T1	T2	T3	T4	T5	T6	T7	T8	T9	T10	T11	T12	Depth	Tilt	Water T	Int. T
62	610.0	1455.3	1385.5	1311.5	1237.9	1189.8	1128.9	1063.3	996.5	948.9	891.0	829.3	762.4	-1880.3	4.0	-1514.0	281.6
63	620.0	1456.7	1386.5	1312.4	1235.2	1189.4	1124.4	1062.4	997.9	947.6	892.4	825.7	764.2	-1880.1	8.0	-1514.8	285.3
64	630.0	1453.0	1390.5	1314.2	1238.3	1191.6	1127.0	1068.2	999.1	948.0	893.7	829.7	763.3	-1880.6	4.0	-1510.6	287.1
65	640.0	1452.7	1386.1	1313.0	1236.6	1189.4	1126.7	1063.8	997.9	948.1	891.5	827.2	762.9	-1879.5	4.0	-1513.2	288.7
66	650.0	1454.5	1387.9	1312.9	1237.5	1189.0	1124.4	1066.9	997.0	946.7	892.0	826.7	760.7	-1879.8	4.0	-1514.5	292.4
67	660.0	1455.3	1388.3	1312.9	1237.0	1190.7	1127.1	1065.5	1001.4	946.7	891.5	827.5	761.5	-1880.6	4.0	-1512.3	293.3
68	670.0	1454.0	1389.7	1312.9	1234.3	1187.6	1125.8	1065.6	997.9	946.7	890.2	826.7	761.5	-1880.6	4.0	-1513.2	297.1
69	680.0	1451.7	1387.5	1312.5	1238.0	1191.3	1126.7	1063.4	997.5	945.8	887.0	825.4	763.3	-1879.5	4.0	-1514.5	298.1
70	690.0	1450.4	1388.4	1314.4	1234.4	1189.9	1127.2	1062.4	1000.1	947.6	888.8	828.0	759.3	-1880.3	4.0	-1511.1	303.3
71	700.0	1449.1	1387.6	1308.5	1236.3	1186.8	1124.1	1064.3	994.4	947.7	888.0	823.6	762.1	-1880.3	4.0	-1516.6	305.8
72	710.0	1451.2	1385.9	1312.8	1236.5	1194.8	1131.1	1068.2	1001.0	951.2	893.2	829.7	764.2	-1880.3	8.0	-1513.5	307.3
73	720.0	1456.3	1385.1	1311.1	1236.6	1192.2	1129.4	1062.4	996.1	946.7	892.8	827.6	759.8	-1881.2	4.0	-1512.3	309.3
74	730.0	1453.3	1385.8	1310.3	1234.5	1187.3	1122.3	1061.2	996.6	944.6	888.9	825.0	759.4	-1880.1	4.0	-1513.2	311.9
75	740.0	1450.9	1385.7	1314.8	1235.3	1187.2	1122.2	1064.3	998.8	947.7	888.4	824.9	762.5	-1880.1	4.0	-1509.8	315.5
76	750.0	1452.6	1387.9	1312.4	1236.1	1188.9	1123.5	1062.4	996.5	945.3	888.4	825.3	759.7	-1880.3	4.0	-1512.7	317.7
77	760.0	1476.7	1379.7	1308.0	1549.9	1305.3	2210.9	1835.8	1332.7	2044.1	1771.4	1979.8	1169.9	-1880.6	4.0	-1518.3	311.8
78	770.0	8626.1	4663.2	4581.0	7065.8	6148.4	8575.0	6044.2	5383.6	6819.3	6012.2	5926.0	4256.6	-1881.4	4.0	-1510.2	323.8
79	780.0	3969.5	3214.6	2988.7	3322.5	3066.7	3651.7	3073.9	2924.9	3192.6	2912.3	2745.8	2336.5	-1879.8	4.0	-1514.4	325.3
80	790.0	2550.1	2271.7	2148.1	2198.6	2130.8	2251.8	2023.3	1941.2	2023.0	1876.9	1741.1	1615.5	-1880.9	4.0	-1511.8	329.2
81	800.0	2056.2	1901.8	1818.2	1796.6	1777.0	1770.0	1641.2	1580.5	1582.8	1489.8	1386.7	1318.2	-1880.6	4.0	-1510.7	330.5
82	810.0	1857.4	1742.5	1674.7	1628.9	1615.6	1571.2	1479.2	1421.9	1392.9	1321.4	1234.5	1177.1	-1880.1	8.0	-1514.9	333.7
83	820.0	1761.6	1664.0	1597.0	1542.4	1529.3	1474.7	1395.3	1339.0	1294.4	1232.7	1151.2	1095.5	-1880.9	4.0	-1509.8	337.0
84	830.0	1703.2	1614.0	1551.9	1491.0	1473.8	1410.1	1339.3	1286.1	1232.1	1176.7	1102.6	1043.1	-1880.3	4.0	-1514.0	341.2
85	840.0	1668.6	1585.8	1518.7	1458.0	1434.9	1374.1	1300.3	1249.1	1193.6	1140.4	1064.1	1010.5	-1880.1	8.0	-1507.6	341.5
86	850.0	1641.1	1558.2	1490.8	1423.8	1406.3	1341.8	1270.0	1215.3	1162.4	1108.9	1034.5	975.2	-1880.3	4.0	-1511.5	343.9
87	860.0	1622.8	1542.2	1478.1	1408.9	1386.8	1320.5	1255.2	1199.3	1143.2	1089.3	1013.7	955.8	-1879.2	4.0	-1514.0	344.6
88	870.0	1601.9	1526.4	1461.4	1391.4	1369.4	1297.1	1234.3	1179.9	1121.4	1067.6	1000.2	938.7	-1881.4	4.0	-1510.7	351.2
89	880.0	1593.4	1511.4	1450.6	1376.1	1353.2	1283.7	1224.1	1161.6	1107.6	1054.4	983.4	927.0	-1879.5	4.0	-1507.6	349.5
90	890.0	1577.8	1500.9	1435.1	1367.6	1339.6	1273.4	1208.8	1149.6	1092.3	1037.9	969.6	911.4	-1880.9	4.0	-1513.2	351.7
91	900.0	1570.8	1492.0	1428.1	1357.4	1326.3	1258.7	1197.4	1139.6	1084.6	1029.3	959.2	899.8	-1878.7	4.0	-1512.8	354.5
92	910.0	1562.6	1487.0	1421.7	1349.7	1318.6	1251.0	1189.3	1129.3	1074.2	1021.2	952.1	890.8	-1879.8	4.0	-1511.5	358.3
93	920.0	1556.0	1482.3	1413.3	1342.7	1310.3	1243.2	1181.9	1122.5	1067.8	1012.2	945.3	885.4	-1881.2	4.0	-1511.1	361.1
94	930.0	1548.5	1475.3	1408.7	1336.7	1304.2	1235.8	1176.0	1115.6	1060.5	1005.4	938.5	880.0	-1880.1	4.0	-1510.2	363.8
95	940.0	1544.4	1471.6	1402.2	1330.8	1296.1	1229.5	1168.8	1108.2	1056.0	998.7	932.2	868.9	-1880.9	8.0	-1510.2	366.7
96	950.0	1539.4	1467.5	1398.1	1323.9	1292.0	1226.3	1163.8	1103.5	1051.0	992.4	924.6	864.4	-1880.9	4.0	-1511.1	370.0
97	960.0	1535.6	1462.7	1394.3	1320.6	1288.3	1220.3	1162.8	1099.4	1045.5	990.5	924.1	859.5	-1879.8	4.0	-1508.5	372.3
98	970.0	1528.3	1457.3	1390.8	1316.2	1278.8	1215.9	1152.5	1090.9	1039.3	981.2	916.2	853.7	-1880.3	4.0	-1509.4	370.6
99	980.0	1529.1	1456.3	1386.0	1315.6	1278.2	1211.2	1153.3	1087.7	1036.9	981.6	913.9	851.0	-1879.0	4.0	-1511.9	377.0
100	990.0	1526.7	1455.2	1386.8	1314.2	1276.7	1208.8	1150.1	1088.5	1033.7	974.3	910.2	846.9	-1881.7	4.0	-1506.3	380.6
101	1000.0	1520.4	1450.7	1382.8	1306.0	1272.7	1205.3	1143.8	1081.0	1029.3	974.4	906.2	845.6	-1881.4	4.0	-1506.4	380.3
102	1010.0	1514.2	1445.5	1373.0	1303.1	1262.0	1198.3	1138.1	1073.0	1022.7	964.2	901.9	836.9	-1881.7	4.0	-1515.0	381.7
103	1020.0	1515.9	1446.7	1376.5	1302.0	1262.8	1194.9	1138.0	1075.6	1020.7	968.6	900.9	838.1	-1881.7	4.0	-1511.1	383.7
104	1030.0	1510.7	1441.5	1375.0	1299.2	1259.0	1192.6	1133.4	1073.3	1019.3	962.7	896.4	834.1	-1880.9	4.0	-1510.2	388.8
105	1040.0	1510.8	1441.1	1371.0	1296.1	1256.9	1193.1	1130.7	1068.9	1015.3	959.6	893.7	831.9	-1880.6	4.0	-1509.4	389.9
106	1050.0	1509.4	1436.0	1368.2	1292.8	1254.6	1190.8	1127.1	1068.0	1012.6	957.8	891.9	828.7	-1880.3	4.0	-1510.7	393.2
107	1060.0	1503.8	1433.7	1366.8	1292.4	1254.1	1186.7	1126.6	1061.2	1010.8	953.8	889.7	827.4	-1879.8	4.0	-1509.0	393.6
108	1070.0	1502.9	1432.4	1364.5	1289.7	1250.9	1184.5	1124.4	1062.1	1006.3	952.9	887.0	823.4	-1880.9	4.0	-1511.5	395.5
109	1080.0	1504.8	1430.9	1360.4	1288.3	1247.8	1183.6	1122.6	1058.5	1005.4	949.8	884.3	823.0	-1882.2	4.0	-1511.9	396.0
110	1090.0	1504.6	1432.6	1363.0	1287.2	1249.4	1183.0	1125.6	1063.8	1008.9	951.5	884.3	822.0	-1878.7	4.0	-1508.5	402.4
111	1100.0	1499.1	1431.3	1358.4	1288.2	1245.8	1181.2	1121.6	1054.4	1005.8	947.0	885.2	818.5	-1884.1	4.0	-1506.0	404.8
112	1110.0	1503.2	1433.0	1358.3	1286.2	1248.0	1181.5	1116.5	1057.1	1005.7	948.8	882.0	817.5	-1884.4	4.0	-1507.2	405.1
113	1120.0	1497.0	1426.4	1356.7	1282.4	1244.6	1176.3	1112.7	1049.5	998.2	940.4	877.2	816.3	-1884.7	4.0	-1508.5	406.9
114	1130.0	1497.9	1426.4	1354.9	1282.8	1238.2	1173.6	1115.8	1050.5	1000.4	940.4	879.0	812.8	-1883.6	4.0	-1508.1	409.3
115	1140.0	1495.3	1428.8	1356.9	1279.4	1243.5	1177.5	1116.5	1052.1	999.8	945.1	879.3	814.9	-1876.5	4.0	-1508.1	413.1
116	1150.0	1494.0	1424.8	1355.2	1279.9	1237.6	1171.1	1113.0	1048.6	997.2	941.2	875.8	813.1	-1878.7	4.0	-1507.2	415.2
117	1160.0	1491.5	1425.0	1351.7	1278.3	1238.7	1169.5	1108.6	1049.1	994.6	936.8	873.2	809.6	-1883.1	8.0	-1509.0	415.5
118	1170.0	1493.1	1422.5	1353.8	1279.5	1236.7	1172.5	1109.4	1051.7	993.6	940.3	874.0	810.9	-1879.8	4.0	-1506.8	420.3
119	1180.0	1491.4	1420.2	1352.5	1276.3	1234.9	1169.8	1109.9	1046.8	992.7	936.7	872.2	808.7	-1880.6	4.0	-1508.1	423.3
120	1190.0	1488.1	1417.9	1350.2	1275.9	1233.1	1164.9	1106.3	1047.3	991.8	935.4	870.9	805.5	-1880.6	4.0	-1508.1	423.3
121	1200.0	1490.0	1419.4	1348.8	1274.1	1232.2	1166.7	1107.2	1043.7	990.9	935.0	870.0	805.5	-1880.3	4.0	-1508.1	426.1
122	1210.0	1485.9	1416.6	1348.8	1275.0	1233.1	1164.0	1103.1	1039.6	988.7	932.7	869.6	806.0	-1880.1	4.0	-1507.7	428.1

Table 2 Station 4p4 data corrected for appropriate units; temperature in mili-degree C, depth in meter, tilt in degree (2/3).

	time	T1	T2	T3	T4	T5	T6	T7	T8	T9	T10	T11	T12	Depth	Tilt	Water T	Int. T
123	1220.0	1487.1	1418.8	1346.9	1274.0	1232.6	1166.6	1104.9	1040.0	990.4	935.4	867.3	805.5	-1880.9	4.0	-1506.8	432.7
124	1230.0	1484.1	1417.1	1343.8	1272.3	1228.2	1163.6	1105.0	1036.5	988.2	927.8	863.8	803.4	-1880.3	4.0	-1506.4	432.9
125	1240.0	1487.6	1416.0	1345.5	1270.8	1227.6	1165.7	1106.7	1044.1	991.8	933.1	868.6	804.2	-1879.8	4.0	-1507.7	435.0
126	1250.0	1477.7	1412.5	1346.2	1266.0	1224.1	1160.4	1101.4	1035.6	986.0	926.0	860.7	801.2	-1881.2	8.0	-1511.5	435.8
127	1260.0	1486.3	1412.8	1343.7	1271.8	1227.6	1156.6	1103.5	1038.7	983.7	929.6	865.5	798.9	-1881.7	8.0	-1505.1	436.0
128	1270.0	1479.1	1409.8	1341.1	1265.5	1222.7	1155.0	1097.3	1032.9	980.2	925.6	863.4	798.1	-1880.6	4.0	-1507.7	439.1
129	1280.0	1484.9	1414.7	1343.7	1269.9	1228.1	1158.4	1103.1	1037.8	985.4	928.6	862.4	799.7	-1880.6	4.0	-1506.8	444.5
130	1290.0	1481.6	1414.7	1343.7	1267.7	1225.4	1156.6	1098.5	1036.5	981.4	926.9	862.9	799.3	-1878.2	4.0	-1504.3	444.5
131	1300.0	1479.8	1412.4	1341.5	1267.2	1223.6	1156.2	1097.7	1033.8	982.3	926.4	863.3	798.5	-1881.7	4.0	-1506.4	447.9
132	1310.0	1480.8	1413.3	1341.9	1264.5	1225.8	1154.8	1097.2	1036.5	981.9	924.2	861.1	796.2	-1881.4	8.0	-1505.6	449.3
133	1320.0	1477.3	1408.0	1341.2	1262.8	1221.9	1155.5	1095.6	1030.3	980.2	922.0	856.2	795.0	-1880.6	4.0	-1505.2	449.6
134	1330.0	1478.9	1409.6	1340.5	1264.9	1222.2	1153.9	1099.0	1035.1	981.9	927.3	862.4	798.9	-1880.3	8.0	-1506.0	454.0
135	1340.0	1475.5	1409.0	1333.9	1263.8	1217.9	1149.6	1093.8	1029.4	977.6	919.9	857.2	790.1	-1880.3	4.0	-1510.3	452.1
136	1350.0	1474.9	1403.3	1337.0	1263.7	1218.2	1147.7	1094.6	1032.1	977.9	918.4	854.9	792.3	-1880.1	4.0	-1508.1	451.9
137	1360.0	1476.6	1405.5	1339.2	1264.1	1220.4	1153.1	1096.3	1029.3	977.0	917.9	858.4	794.0	-1880.9	4.0	-1505.6	459.3
138	1370.0	1480.7	1407.2	1340.0	1261.2	1222.1	1151.2	1096.3	1032.4	977.3	923.7	858.5	798.6	-1880.3	4.0	-1502.6	460.1
139	1380.0	1475.2	1405.9	1338.2	1264.0	1219.0	1149.4	1091.8	1027.5	977.3	922.8	857.9	794.0	-1881.4	4.0	-1505.6	463.9
140	1390.0	1476.6	1405.0	1335.1	1261.8	1220.0	1148.5	1092.7	1028.9	977.0	921.5	855.7	789.6	-1881.4	8.0	-1506.4	465.9
141	1400.0	1476.6	1406.0	1336.0	1261.3	1216.7	1149.0	1089.6	1028.9	974.2	918.8	855.7	791.8	-1878.7	4.0	-1503.4	465.9
142	1410.0	1474.4	1405.1	1337.4	1260.4	1218.2	1148.1	1090.9	1026.6	975.6	918.8	855.7	791.8	-1880.1	4.0	-1506.4	467.9
143	1420.0	1474.4	1405.1	1335.6	1260.9	1215.4	1148.6	1090.1	1027.5	975.6	918.0	854.4	791.4	-1881.4	4.0	-1504.8	467.4
144	1430.0	1474.4	1404.1	1336.0	1259.9	1215.9	1147.6	1090.9	1025.7	975.6	918.4	854.4	790.4	-1879.2	4.0	-1507.7	472.6
145	1440.0	1472.2	1404.8	1335.2	1257.8	1213.3	1143.7	1086.5	1022.2	971.2	915.3	851.4	788.8	-1880.9	4.0	-1506.5	472.4
146	1450.0	1471.3	1404.8	1330.7	1256.5	1216.0	1141.4	1088.3	1025.4	971.7	916.2	850.9	790.1	-1881.7	4.0	-1507.8	473.8
147	1460.0	1470.8	1402.9	1334.7	1255.9	1212.3	1145.9	1086.9	1022.2	973.4	917.1	850.4	786.0	-1881.2	4.0	-1504.3	473.7
148	1470.0	1472.6	1403.3	1333.7	1258.2	1214.1	1145.4	1088.3	1025.3	971.6	917.5	854.9	790.5	-1879.8	4.0	-1506.9	481.6
149	1480.0	1470.6	1404.5	1335.0	1258.0	1216.7	1142.1	1090.9	1023.0	974.2	914.8	855.3	788.6	-1880.1	4.0	-1503.9	480.5
150	1490.0	1472.9	1402.7	1332.7	1258.5	1216.3	1146.7	1090.5	1023.0	972.4	917.0	853.9	791.3	-1879.2	4.0	-1503.0	485.3
151	1500.0	1471.1	1403.2	1335.0	1257.6	1214.5	1142.6	1088.2	1027.1	972.4	916.6	851.7	786.9	-1881.4	4.0	-1508.1	485.3
152	1510.0	1471.6	1404.6	1332.8	1259.0	1212.7	1141.7	1087.3	1021.2	973.8	914.4	852.6	788.2	-1881.4	4.0	-1508.1	487.7
153	1520.0	1470.3	1402.3	1331.0	1255.9	1210.9	1142.7	1086.5	1023.1	970.7	913.5	849.9	786.5	-1881.2	4.0	-1512.4	488.7
154	1530.0	1468.9	1403.3	1331.9	1255.4	1212.3	1138.6	1083.3	1023.5	970.7	911.2	850.8	786.5	-1881.4	4.0	-1508.5	489.2
155	1540.0	1467.5	1400.1	1332.8	1254.5	1208.6	1142.2	1086.9	1021.7	968.9	913.0	850.9	785.2	-1881.2	4.0	-1511.1	488.8
156	1550.0	1469.3	1402.7	1333.2	1257.2	1211.7	1142.6	1083.7	1018.5	967.5	912.1	850.8	787.3	-1880.6	8.0	-1511.5	495.3
157	1560.0	1468.6	1396.5	1331.5	1251.4	1209.6	1138.2	1085.2	1016.4	968.0	911.3	848.2	781.6	-1882.8	4.0	-1509.5	493.2
158	1570.0	1469.9	1400.6	1330.6	1250.5	1204.6	1134.6	1083.8	1019.9	968.9	908.6	844.6	780.7	-1882.2	8.0	-1515.0	493.1
159	1580.0	1503.4	1424.1	1334.2	1248.6	1240.0	1167.7	1092.3	1015.0	983.3	900.0	806.7	749.6	-1879.8	8.0	-1514.5	499.7
160	1590.0	1292.5	1231.4	1179.0	1010.2	935.5	823.7	747.7	675.1	604.0	524.3	428.0	369.0	-1877.6	13.0	-1512.4	498.2
161	1600.0	744.5	738.5	690.6	498.2	343.6	304.4	266.7	274.4	221.4	190.7	150.6	138.1	-1876.5	8.0	-1513.3	497.5
162	1610.0	246.7	249.4	245.8	171.5	106.1	92.3	78.4	99.4	73.0	63.2	48.8	46.2	-1873.8	4.0	-1510.7	504.2
163	1620.0	69.7	69.0	68.5	49.1	23.8	22.2	17.8	21.2	20.7	18.8	13.4	16.3	-1871.4	4.0	-1512.0	503.5
164	1630.0	15.3	16.8	15.1	12.4	-0.1	-1.2	-1.8	0.4	4.5	3.5	3.1	2.2	-1868.1	4.0	-1514.6	503.7
165	1640.0	0.9	2.3	2.7	-0.3	-5.1	-3.8	-6.0	-4.7	1.9	1.8	0.6	1.8	-1866.2	4.0	-1511.5	507.4
166	1650.0	-2.5	-3.2	-3.2	-4.6	-5.1	-5.0	-7.3	-7.2	-1.9	2.2	4.0	-1.1	-1866.2	4.0	-1515.0	508.8
167	1660.0	-5.0	-9.2	-2.4	-5.4	-9.4	-7.2	-9.8	-6.8	-1.0	-1.2	1.4	-0.3	-1863.7	4.0	-1515.0	512.7
168	1670.0	-9.7	-9.2	-7.5	-6.7	-11.5	-11.8	-10.2	-11.4	-3.2	-2.0	-1.5	-2.4	-1855.6	4.0	-1512.8	512.5
169	1680.0	-5.9	-4.5	-5.4	-4.1	-9.8	-5.9	-9.4	-5.5	-3.6	-0.3	-0.2	0.6	-1845.2	4.0	-1512.8	513.5
170	1690.0	-4.6	-5.4	-3.6	-0.7	-5.5	-8.4	-7.7	-4.7	-0.6	-0.7	4.5	3.6	-1830.6	4.0	-1512.4	521.5
171	1700.0	-5.0	-8.7	-5.7	-2.0	-8.1	-8.8	-7.7	-4.2	-1.9	-0.3	0.6	2.3	-1819.7	4.0	-1523.4	521.9
172	1710.0	-7.5	-6.2	-4.5	-1.6	-9.0	-8.4	-9.4	-8.0	-2.3	0.1	0.2	-2.0	-1811.2	4.0	-1525.9	523.5
173	1720.0	-9.7	-6.2	-5.3	-4.5	-7.7	-8.0	-7.7	-8.0	-2.3	0.5	-0.7	-0.7	-1797.1	4.0	-1527.6	523.0
174	1730.0	-10.1	-9.2	-6.2	-3.7	-9.4	-6.7	-9.8	-8.0	-3.2	-1.6	-0.7	0.1	-1788.1	4.0	-1530.2	525.4
175	1740.0	-8.4	-8.3	-5.8	-3.7	-10.2	-9.7	-5.6	-8.4	-4.0	-0.3	1.5	1.0	-1775.9	4.0	-1528.5	526.7
176	1750.0	-6.3	-7.1	-6.2	-5.8	-10.7	-8.0	-6.4	-6.4	-2.8	-1.6	-1.9	-1.6	-1766.4	4.0	-1529.3	527.8
177	1760.0	-10.1	-12.7	-7.9	-8.8	-10.7	-11.4	-12.0	-9.0	-6.2	-2.1	-4.1	-3.7	-1754.4	4.0	-1532.8	529.9
178	1770.0	-10.1	-10.5	-8.8	-7.5	-12.0	-13.1	-12.8	-11.5	-5.7	-4.2	-3.2	-4.1	-1743.2	4.0	-1533.2	528.3
179	1780.0	-13.1	-10.1	-4.9	-8.4	-9.8	-15.3	-11.1	-8.5	-6.2	-2.5	-3.7	-1.2	-1733.7	4.0	-1529.8	528.4

Table 2 Station 4p4 data corrected for appropriate units; temperature in mili-degree C, depth in meter, tilt in degree (3/3).

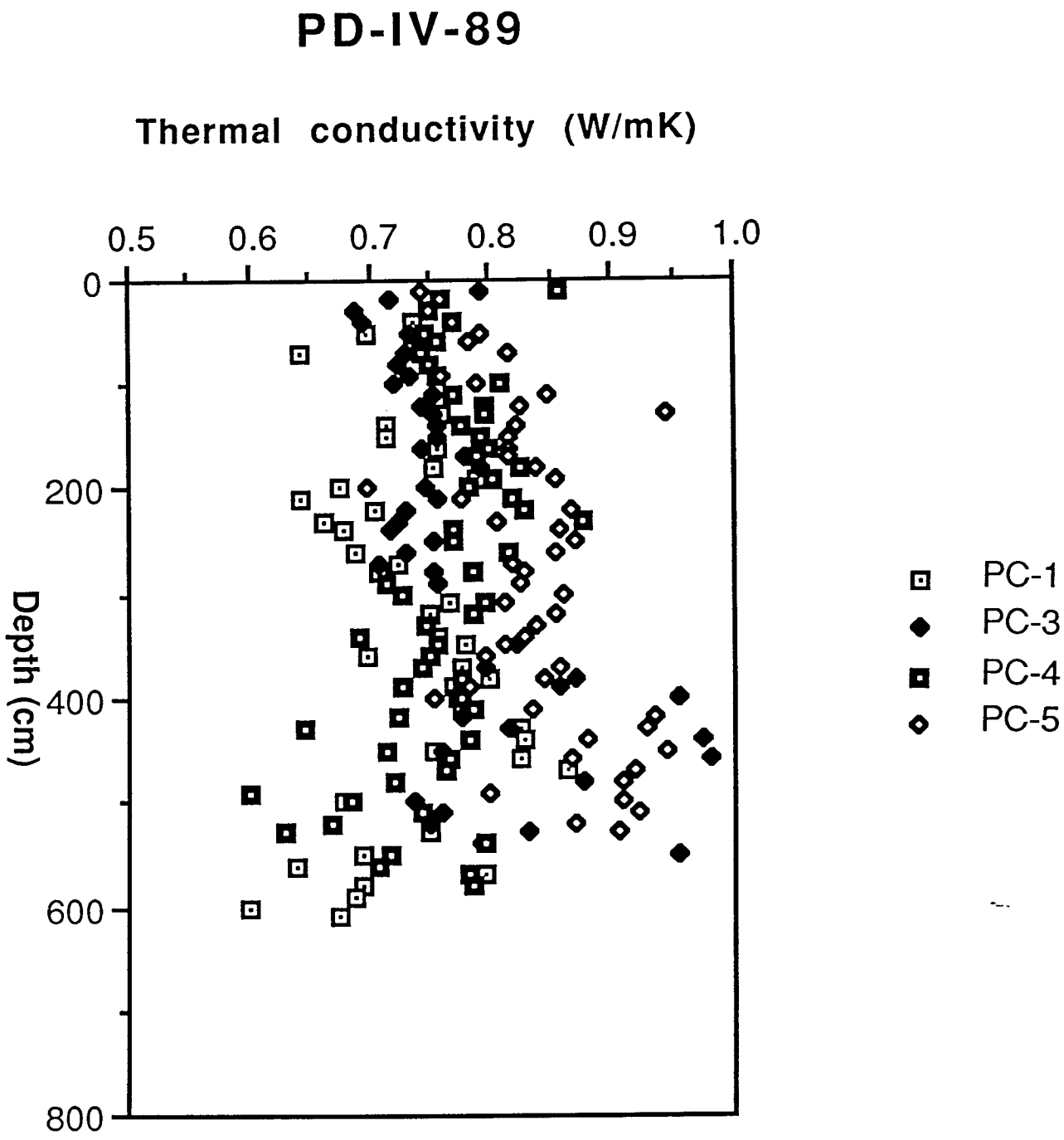

Fig. 7 Thermal conductivity data measured on the piston core samples on PD-IV-89 cruise.

Villinger and Davis, 1987a) whereas our probe is thinner (6.35 mm diam.) than the other's (10 mm diam.). The similarity of the shifts are probably due to our heater power being only 1/3 to 1/4 of that of the violin-bow. For the 10 sec. pulse case, the shift values are much shorter while the heater power is still 1/2. Thus, with heater power more than 300 J/m, we could make the in-situ conductivity measurements with much less origin time shift. The required power is still half that of the violin-bow probe. We do not see any depth dependence of the origin time shift as reported by Villinger and Davis (1987a). The short sensor string probably solved the contact resistance problem caused by the long pull-through length of the violin-bow probe.

5. Discussion of results

Table 4 shows the heat flow values, errors, depths of super-penetration, and unused sensors for the heat flow calculation. For the stations without in-situ thermal conductivity, a constant conductivity at depth (0.765 W/mK) was assumed. Means of the standard errors from the best fit to the Bullard plot/thermal gradient plot are 1.2 % for the in-situ conductivity stations and 2.0 % for the non-in-situ conductivity stations, both at the 90 % confidence level. The values are comparable or even better than the accuracy that Lister et al. (1989) achieved (0.5 to 3.0 %) using a violin-bow probe. Apparently, the increased number of individual temperature measurements is beneficial; we had twelve thermistors while Lister et al. (1989) had seven.

Sixteen of the 54 penetrations show a low-temperature deviation for uppermost sensor #12 from the best fit line on the Bullard plot or the thermal gradient plot (Fig. 8). Most of such penetrations also show that the similar deviation for lowermost sensor #1. If there is a sharp or/and frequent thermal conductivity variation at depth, the Bullard plot may not cancel the effect of and show non-linearity. The piston core samples recovered in the King George Basin show that there is a high-conductivity ash layer (0.2 to 0.3 m thick) at 0.5 to 1.5 m depth. If this is the cause (at least for #12), the deviation should be observed around the same sub-bottom depth. However, the estimated super penetration depths (Table 4) indicate that the #12 sensor was, in

	T1 (bottom)	T2	T3	T4	T5	T6	T7	T8	T9	T10	T11	T12 (top)
10 sec	Q=260.1				Q=299.6							
1p1	12.2	9.1	9.4	12.3	12.4	14.6	13.1	11.3				
8 sec	Q=208.0				Q=239.7				Q=251.6			
2p1	26.7	27.4	26.1	27.4	23.6	28.5	26.9	27.7	21.7	22.1	21.3	22.0
2p2	23.1	26.1	22.1	24.2	22.2	25.8	22.7	25.1	22.0	20.2	20.1	21.1
2p4	23.6	24.8	22.7	25.1	23.9	26.6	21.8	22.1	22.0	19.3	20.4	18.2
2p5	23.3	21.8	22.2	23.0	19.3	21.3	19.8	22.6	19.5	18.5	17.3	17.1
8p1	27.0	24.9	22.9	24.2	24.7	26.6	24.4	25.3	21.6	20.1	18.8	19.7
8p3	25.0	23.5	21.8	21.9	22.8	21.7	21.3	22.5	21.0	19.8	18.2	19.2
8p8	17.0	16.1	16.8	21.2	15.4	19.6	20.4	15.4	16.9	17.6	14.9	15.7
average	23.7	23.5	22.1	23.9	21.7	24.3	22.5	23.0	20.7	19.7	18.7	19.0
S.D.	3.3	3.7	2.7	2.1	3.3	3.4	2.5	3.9	1.9	1.4	2.2	2.2
6 sec	Q=156.1				Q=179.7				Q=188.7			
3p2	24.2	26.0	23.0	26.5	22.6	27.2	21.6	24.6	23.6	19.6	20.9	22.2
4p1	24.9	24.8	23.0	26.2	23.9	26.9	25.3	24.3	23.7	20.2	18.1	25.2
4p3	26.6	24.8	22.2	25.3	23.2	23.6	21.0	24.7	20.4	20.7	21.9	19.6
4p4	25.7	21.1	23.1	24.1	25.8	27.4	22.7	24.6	19.6	19.8	17.0	18.4
4p5	15.6	15.7	17.1	19.3	17.5	17.2	13.7	17.9	16.5	13.6	12.5	17.9
5p3	35.7	30.9	27.8	30.3	30.2	30.9	28.0	30.9	29.8	25.7	24.3	24.6
5p4	23.9	24.0	20.1	26.3	22.2	25.0	23.5	21.7	20.2	18.0	18.1	18.0
6p2	26.2	23.9	23.7	26.2	24.3	26.0	23.4	23.2	22.4	20.7	22.3	18.8
6p3	25.3	25.4	22.5	26.8	22.9	26.2	24.7	23.6	23.0	20.2	19.4	18.2
6p4	31.5	30.3	26.5	25.9	28.0	30.1	28.1	29.3	37.3	19.2	16.6	19.7
6p5	18.0	16.1	16.5	18.9	15.3	16.8	15.1	34.2	17.7	16.0	14.6	17.1
average	25.2	23.9	22.3	25.1	23.3	25.2	22.5	25.4	23.1	19.4	18.7	20.0
S.D.	5.5	4.8	3.4	3.3	4.2	4.6	4.6	4.5	5.9	3.0	3.5	2.8

Table 3 Heat pulse origin time (sec) shift at each sensor for the in-situ thermal conductivity determination.

station	super-penet.	heat flow	No. sen. used	unused sen.	heat pulse	error (%)
1.1		114	6	1,8	Y	1.3
1.2		193	8			1.8
1.3		124	6	1,8		4.2
1.4		421	6	4,5		3.3
2.1	2.76	219	10	1,12	Y	1.4
2.2	2.93	105	10	1,12	Y	0.6
2.3	3.57	31	11	1		2.7
2.4	2.83	128	10	1,12	Y	1.2
2.5	3.40	118	11	1	Y	0.9
2.6	2.52	81	12			1.6
2.7		68	8	5,6,7,8		2.8
3.1	2.48	168	12			1.8
3.2	2.84	139	10	1,12	Y	1.2
3.3	3.21	174	12			1.0
3.4	2.45	112	11	7		2.9
3.5	2.49	55	12			1.7
3.6		72	8			3.6
3.7	2.35	68	8	1,2,3,4		1.6
3.8	2.70	129	10	1,12		3.5
4.1	3.05	145	9	2,3,12	Y	1.5
4.2	3.34	225	11	11		1.9
4.3	2.77	176	10	1,12	Y	1.0
4.4	3.06	184	12		Y	0.9
4.5	2.57	111	7	5,6,7,8,9	Y	0.7
5.1	3.13	94	9	1,8,12		2.5
5.2	3.38	143	12			1.4
5.3	3.07	114	11	12	Y	0.9
5.4	3.07	104	11	12	Y	1.2
5.5	3.35	174	12			2.6
5.6	2.46	142	7	1,2,3,4,10		1.4
5.7	3.22	101	10	4,12		2.3
6.1	2.78	127	11	11		1.6
6.2	3.39	186	11	12	Y	1.2
6.3	3.25	140	10	1,12	Y	0.7
6.4	3.03	93	11	9	Y	0.8
6.5	2.56	148	8	5,6,7,8	Y	1.7
7.1	3.12	118	12			1.6
7.2	3.09	87	12			1.0
7.3	3.34	98	12			1.2
7.4	2.70	91	11	8		1.3
7.5		99	8			3.9
7.6	2.56	95	8	5,6,7,8		1.2
7.7	2.40	99	8	5,6,7,8		1.1
7.8	2.20	115	8	5,6,7,8		0.8
7.9		251	10			2.2
8.1	2.92	107	9	1,8,12	Y	0.9
8.2	2.19	69	12			2.1
8.3	2.53	46	9	1,8,12	Y	1.6
8.4	3.37	48	12			1.0
8.5	3.34	42	8	5,6,7,8		3.0
8.6	3.06	82	8	5,6,7,8		1.2
8.7	2.96	154	7	4,5,6,7,8		1.2
8.8	1.88	87	9	7,8,12	Y	2.2
8.9		55	7			18.5

Table 4 Heat flow data (mW/m^2) obtained during PD-IV-89 cruise. The super-penetration (m) is the sub-bottom depth of the uppermost sensor. (Error in 90 % confidence level.)

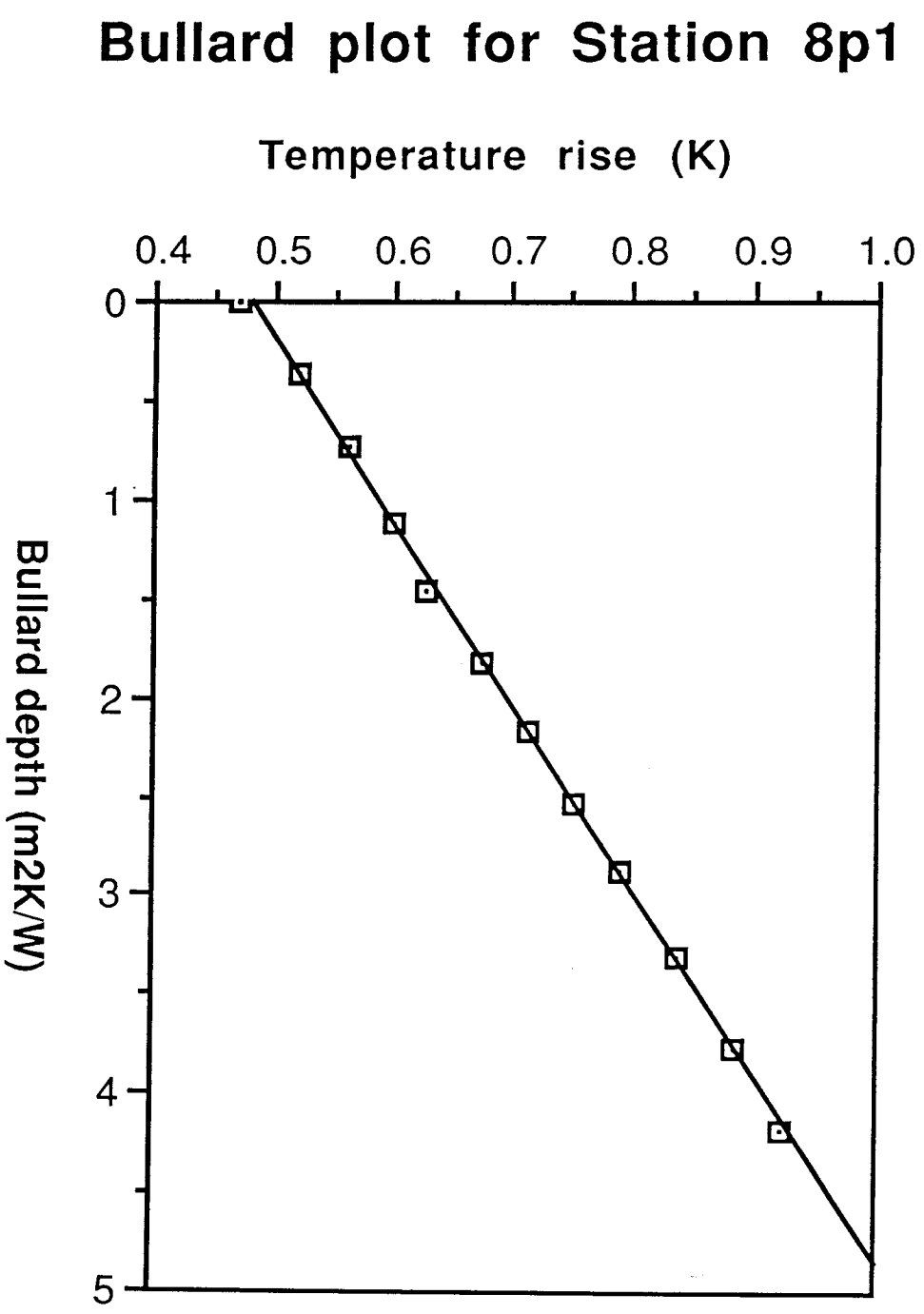

Fig. 8 Bullard Plot showing low-temperature deviation for sensors #1 (lowermost) and #12 (uppermost)

most cases, below 2.5 m sub-bottom depth and there is no correlation to the depth of super penetration with the low-temperature deviation.

Other possible causes are environmental thermal disturbance or mechanical disturbance to the sediments. For example, if the bottom water temperature dropped recently, it could explain the low-temperature deviation of the uppermost sensor. However, if so, all the stations should show the similar temperature deviation. Occurrence of hydrothermal activity is possible in the King George Basin (Nagihara and Lawver, 1989). Fluid migration within sediments often shows up as a convex or concave thermal profile (e.g. Anderson et al., 1979). However, the thermal gradients we obtained are generally linear except at the sensors #1 and #12. Thus, this is probably not the cause of temperature deviation. Lister et al. (1989) reported similar low-temperature deviations of uppermost sensor for their violin-bow probe from measurements in the west Pacific. They pointed out a possibility that there was a wedge of cold sediment ahead of the weight stand when it super penetrated and that the cold sediment affected the uppermost thermistor. This explanation might apply to our #12 sensor. However, the deviation for the #1 sensor remains unsolved. It is possible that there was some kind of mechanical disturbance around the #1 sensor since it mostly coincides when the #12 is disturbed. We plan to try different bottom probe designs and to vary the distance between the nose cone and the bottom sensor which may suggest the solution to the problem.

Seven penetrations show that all 4 of the thermistors in the middle bow have a slight high-temperature offset. This occurred successively along a series of penetrations (Station7p6 through 7p8 and Station 8p5 through 8p7). It is highly possible that the screw applying tension to the bow was loosened and that the bow slid along the strength member during the series of penetrations. The way to apply the tension may need to be reviewed.

CONCLUSIONS

The multi-outrigger-bow marine heat flow instrumentation combines precision with efficiency of the measurement. The use of multiple sensor strings of intermediate length allows for more thermistors than previous probe designs without requiring a thick sensor tube. The assembly is advantageous in the following aspects:

(1) The increased number of individual temperature measurements statistically improve the accuracy of the data.

(2) The thin sensor string reduces the necessary heat pulse power and thus enables more measurements with the same battery capacity.

(3) The short sensor string reduces the pull-through length in the sediments and causes less contact resistance to the sediments.

(4) The short sensor strings make mobilization and assembly of the equipment easy.

Acknowledgements

We are grateful for the very valuable technical support provided by D. Newman and L. Berod at Applied Microsystems Ltd. System integrity of our heat flow probe was tested for the first time on the R/V Gyre of the Texas A&M University as a part of the UTIG student cruise XI lead by E.W. Behrens. Heat flow operations on R/V Polar Duke were greatly assisted by the ship's crew as well as by ITT Antarctic Service personnel. R. Munroe and S. Zellers made the needle probe thermal conductivity measurements on board. The latest version of HFRED was provided by E. Davis at Pacific Geoscience Centre, Canada. This project was funded by National Science Foundation grant DPP86-15307 to L. Lawver and by a Shell Distinguished Professorship to J. Sclater. B. Della Vedova's travel to the University of Texas was supported by NATO.

REFERENCES

Anderson, R. N., Hobart, M. A., and Langseth, M. G., 1979. Convective heat transfer in oceanic crust and sediment in the Indian Ocean. Science, 204, 828-832.

Blackwell, J. H., 1954. A transient flow method for determination of thermal constants of insulating materials in bulk. J. Appl. Phys., 25, 137-144.

Bullard, E. C., 1939. Heat flow in South Africa. Proc. R. Soc. London, A, 173, 474-502.

Bullard, E. C., 1954. The flow of heat through the floor of the Atlantic Ocean, Proc. R. Soc. London, A, 222, 408-429.

Davis, E. E, Lister, C. R. B., and Sclater, J. G., 1984. Towards determining the thermal state of old ocean lithosphere: Heat flow measurements from the Blake-Bahama outer ridge, north-western Atlantic. Geophys. J. R. Astr. Soc., 78, 507-545.

Gerald, R., Langseth, M. G., Jr., and Ewing, M., 1962. Thermal gradient measurements in the water and bottom sediment of the western Pacific, J. Geophys. Res., 67, 785-803.

Hudson R. D., Newman, D. E., Berod, L.D., and Eaton, G. M., 1989. A high resolution geothermal heat probe. Proc. OCEANS '89, 1-6.

Hutchison, I. and Owen, T., 1989. A microprocessor heat flow probe. In:Wright, J. A. and Louden, K. E. (eds.), Handbook of Seafloor Heat Flow, CRC Press, pp 3-70.

Hyndman, R. D., Davis, E. E., and Wright, J. A., 1979. The measurements of marine geothermal heat flow by a multipenetration probe with digital acoustic telemetry and in situ thermal conductivity. Mar. Geophys. Res., 4, 181-205.

Jemsek, J., Von Herzen, R.P., and Andrew, P., 1985. In-situ measurement of thermal conductivity using the continuous-heating line source method and WHOI outrigged probe. Woods Hole Oceanographic Institution Technical Rept., WHOI-85-28, pp 71.

Lister, C. R. B., 1963. Geothermal gradient measurement using a deep sea corer. Geophys. J. R. Astr. Soc., 7, 571-583.

Lister, C. R. B., 1979. The pulse probe method of conductivity measurement. Geophys. J. R.

Astr. Soc., 57, 451-461.

Lister, C. R. B., Davis, E. E., Sclater, J. G., Villinger, H., and Nagihara, S., 1989. Heat flow maintained in ocean basins of great age: investigations in the north-equatorial west Pacific, submitted to Geophys. J. R. Astr. Soc.

Louden, K. E.and Wright, J. A., 1989. Marine heat flow data: a new compilation of observations and brief review of its analysis. In: Wright, J. A. and Louden, K. E. (eds), Handbook of Seafloor Heat Flow, CRC Press, pp 71-90.

Mojesky, T. M., 1981. Rapid in situ thermal conductivity measurements for the study of geothermal heat flow. M.S. thesis, University of Washington.

Nagihara, S. and Lawver, L.A., 1989. Heat flow measurements in the King George Basin, Bransfield Strait, Antarctic J. (in press).

Nagihara, S., Wheeler, J. E., Roberts, A. C., Della Vedova, B., and Lawver, L. A., 1989. Multi-outrigger-bow marine heat flow instrumentation, pt. B: mechanical design, Univ. Texas Inst. Geophys. Tech Rept.

Ratcliffe, E.H., 1960. Thermal conductivities of ocean sediments, J. Geophys. Res., 65, 1535-1541.

Villinger, H. and Davis, E. E., 1987a. A new reduction algorithm for marine heat flow measurements. J. Geophys. Res., 92, 12846-12856.

Villinger, H. and Davis, E. E., 1987b. HFRED: a program for the reduction of marine heat flow data on a microcomputer. Geological Survey of Canada Open File 1627, pp. 78.

Von Herzen, R.P., Cordery, M.J., Detrick, R.S., and Fang, C., 1989. Heat flow and the thermal origin of hot spot swells: the Hawaiian Swells revisited. J. Geophys. Res., 94, 13783-13800.

Von Herzen, R. P. and Maxwell, A. E., 1959. The measurement of thermal conductivity of deep-sea sediments by a needle probe method. J. Geophys. Res., 64, 1557-1563.